Theoretical investigation of the instability of turbulent capillary jets

U. K. Sauerwein

1992

Abstract

While a stability theory has existed for a long time for the laminar capillary jet, there is a lack of theoretical approaches for the turbulent so far. Experimental results point out, however, that the decomposition mechanisms are similar for the laminar and turbulent case. Therefore, an attempt is made to transfer the approaches of the known stability theory, which in its base features goes back to Rayleigh, to the turbulent case. In order to study the effects of turbulence on the rotationally symmetric surface waves relevant in the laminar case, a model is set up that takes into account the coupling between the turbulent apparent stresses and the elongation of the liquid as a result of jet cross-section changes. This coupling is modeled using Batchelor and Proudman's "Rapid Distortion Theory"; however, the derived results are independent in their qualitative statement of this particular turbulence model.

The result of this consideration is that homogeneous turbulence exerts a stabilizing influence on rotationally symmetric surface waves and may even lead to a prevention of this breakup mechanism.

Translator's note: Rough translation from German of: U. K. Sauerwein. "Theoretischer Teil". *Theoretische und experimentelle Untersuchung der Instabilität turbulenter Kapillarstrahlen [Theoretical and experimental investigation of the instability of turbulent capillary jets]*. Darmstadt, Germany: TU Darmstadt, 1992, pp. 16–68. OCLC: 841713740.

The margin indicates the page of the original text. All underlining added by the translator. Underlining indicates phrases for which the exact translation is unclear. The bibliography has been changed to refer to English translations and abstracts of each reference as appropriate.

Translated by Ben Trettel (https://trettel.us/contact.html) via Google Translate and Reverso Context. Last updated on 2020-07-31. SVN revision #2648.

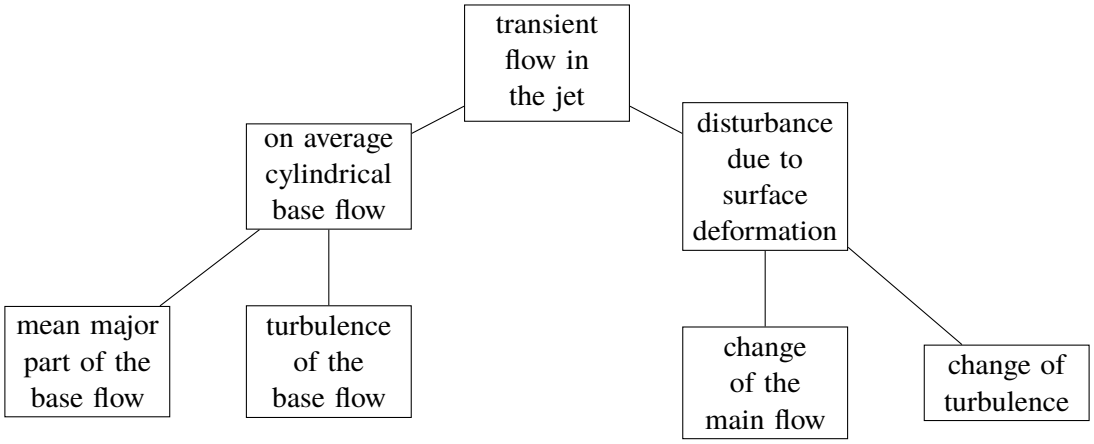

Figure 1: Division into base flow/disturbance as well as main flow/turbulence.

1 Linear spatial stability theory

1.1 Concept and nomenclature

As usual in linear stability theory, the turbulent flow in the capillary jet is divided into a base flow and an (infinitesimally small presumed) disturbance, i.e. deviation from this base flow. In addition, in the turbulent case, there is a distinction between the main flow and the superimposed turbulent fluctuation movement. This gives rise to the scheme sketched in figure 1: The basic flow is turbulent, it has a main flow component, which can be determined by a suitable averaging process, and a turbulent component. The main base flow is constant at purely axial velocity and cylindrical jet surface, thus identical to the undisturbed jet flow already considered by Rayleigh [Ray78]. The turbulence of the base flow is assumed to be homogeneous. If, as a result of a deformation of the jet surface, the main flow deviates from the base solution. This also influences the turbulence structure; their statistical properties are then differentiated by a disturbance component from their base state. Check

p. 16

The definition of the main flow is not entirely unproblematic in the case of the free jet: the velocities resulting from the effect of the surface waves leading to breakup and from the turbulence are superimposed and, indeed, can not be separated at large Reynolds numbers. At intermediate Reynolds numbers, however, the turbulent fluctuations are relatively small and can be observed on the surface of the jet as fine ripples, which are superimposed on much longer-waved surface deformations. The long-wave disturbances are approximately rotationally symmetric and hardly differ from those of a laminar jet.

p. 17

Figure 2 shows a shadow photograph of such a turbulent jet, in which the formation of rotationally

Figure 2: Shadow photograph of a turbulent jet with acoustic stimulation.

symmetric waves was excited by acoustic pressure oscillations. (Further examples can be found in Appendix D.) The line patterns shown are based on light reflections on the turbulence-deformed jet surface.

For the further procedure it is assumed that the discussed separation between disturbances by long-wave surface deformations and by turbulence is possible. This implies the assumption that turbulence length and time scales are much smaller than those of the main flow.

Only mean values in the sense of the usual averaging with unsteady, turbulent flows are considered: If one measures the field size $\varphi(\vec{x}, t)$, one obtains in the i-th measurement at the fixed location $\vec{x}$ and Check at fixed time t (e.g. after starting the process) the measured value $\varphi_i(\vec{x}, t)$. In the limit of infinite repetition of the same measurement, the arithmetic mean of all results tends to the mean values thus Check defined:

$$\overline{\varphi}(\vec{x}, t) := \lim_{N\to\infty} \left[\frac{1}{N} \sum_{i=1}^{N} \varphi_i(\vec{x}, t) \right] (N = \text{number of realizations}). \tag{1}$$

In this type of averaging must be assumed that the main flow is temporally periodic and not stochastic, otherwise the above sum disappears. However, since it has been assumed that the typical time of the p. 18 main flow is much greater than that of the turbulent fluctuations, the mean of (1) can be replaced by averaging over a suitable time interval of realization:[1]

$$\overline{\varphi}(\vec{x}, t) \approx \frac{1}{2T} \int_{t-T}^{t+T} \varphi(\vec{x}, t')\, \mathrm{d}t'. \tag{2}$$

The main value thus defined is independent of the requirement of a periodic main flow and is therefore to be preferred to (1).

In the sense of the linear stability theory, each tensorial field variable F_{ijk}, averaged according to (2), is decomposed into an unperturbed fundamental component (superscript $^{(0)}$) corresponding to the respective size in the absence of surface waves and one resulting from the jet deformation disturbance portion (superscript $^{(1)}$), whereby the identification of the averaging carried out in the following is omitted:

$$F_{ijk} = F^{(0)}_{ijk} + F^{(1)}_{ijk}. \tag{3}$$

[1] See, for example, Bendat and Piersol [BP71, p. 352].

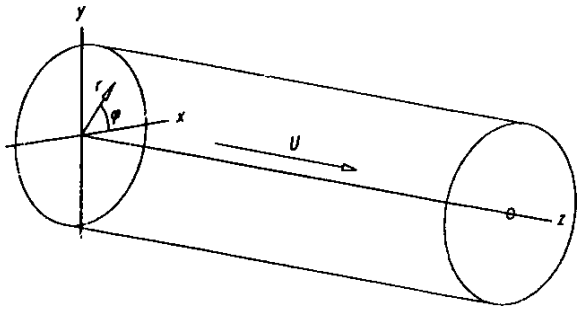

Figure 3: Spatially fixed cylindrical coordinate system.

The coordinate system chosen is the fixed cylindrical coordinate system sketched in figure 3, whose z axis points in the direction of the flow.

Assuming the perturbations as infinitesimal small, they are all proportional to a reference perturbation, for which here the deformation η of the jet radius R p. 19

$$r_s(z,t) = R + \eta. \tag{4}$$

Also, r_s and η are mean values in the sense of (2). Following Rayleigh's result, according to which only rotationally symmetric perturbations are unstable[2], Then η becomes Check

$$r^{(1)} = \eta(z,t) = \mathrm{Re}\left\{\eta_0 \exp[\mathrm{i}k(z-ct)]\right\}, \tag{5}$$

which corresponds to a decomposition in Fourier components. The parameters wavenumber k and phase velocity c are generally complex, so that spatially as well as temporally periodic perturbations Check can be described by a suitable choice of k and c by (5). Again following Rayleigh, it is initially assumed to be purely real k and complex c, i.e., temporally excited, in the jet direction periodic disturbances. This assumption simplifies the subsequent calculation somewhat and is without restriction of generality, since it can be dropped again at any time by setting k as complex. Sec. 2.3 deals with this connection between temporary and convective wave growth.

For the further calculation (5) and the resulting equations are complex extended, so that the identification of the real part Re , which was arbitrarily assigned the physical meaning above, can be dispensed with. Check

[2]An extension of the theory described below to also circumferentially running waves (so-called helical modes) shows that this Rayleigh result remains valid even in the turbulent case (see Prause [Pra88]).

1.2 The Orr-Sommerfeld equation

The stability behavior of the flow in the jet in the case of infinitesimal perturbations can be investigated by means of the Orr-Sommerfeld equation, as is also the case with boundary layer flows. In the problem of boundary layer theory, one is led to an eigenvalue problem due to the homogeneous boundary conditions at the disturbance velocities; the eigenvalue is the complex phase velocity of the wave-like disturbances, the eigenfunctions are current functions of the disturbance velocities.[3] In the case of the liquid jet, the perturbations at the edge of the jet (free surface!) do not have to disappear, the boundary conditions are therefore not homogeneous, and non-trivial solutions of the Orr-Sommerfeld equation are found for all phase velocities. The quantity corresponding to the eigenvalue of the boundary layer problem is defined here by the equilibrium condition at the jet edge. The Orr-Sommerfeld equation should be derived here first for the present problem of a turbulent, on average rotationally symmetric flow.[4] For reasons of symmetry is Check p. 20

$$u_\varphi = \frac{\partial}{\partial \varphi} = 0, \tag{6}$$

so that with an undisturbed base flow with $u^{(0)} = U = \text{const}$ in the z direction the velocity field in

$$u = u^{(0)} + u^{(1)} = U - \frac{1}{r}\frac{\partial \Psi}{\partial r} \text{ (in the } z \text{ direction)}, \tag{7}$$

$$v = v^{(0)} + v^{(1)} = 0 - \frac{1}{r}\frac{\partial \Psi}{\partial r} \text{ (in the } r \text{ direction)}, \tag{8}$$

can be decomposed. The decomposition of the stress tensor, which also includes the turbulent shear stress, into the fundamental and interference component is analogous to Check

$$\tau_{ij} = \tau_{ij}^{(0)} + \tau_{ij}^{(1)}. \tag{9}$$

Inserting (6) through (9) into the Cauchy equation of motion[5] yields the two component equations after deleting the base solution (superscript $^{(0)}$) and neglecting quadratic terms in the disturbance p. 21

[3] See, e.g., Schlichting [Sch87] and Drazin and Reid [DR04].

[4] The calculation procedure described below represents a very unusual application of the Orr-Sommerfeld equation, because here the laminar-turbulent envelope is not investigated, as the base flow is already turbulent!

[5] See Spurk and Aksel [SA10, p. 42].

variables:

$$\frac{\rho}{r}\left[\frac{\partial}{\partial t}+U\,\frac{\partial}{\partial z}\right]\frac{\partial\Psi}{\partial z}=\frac{1}{r}\tau_{rr}^{(1)}+\frac{\partial}{\partial r}\,(\tau_{rr}^{(1)})+\frac{\partial}{\partial z}\,(\tau_{zz}^{(1)})-\frac{1}{r}\tau_{\varphi\varphi}^{(1)}, \tag{10}$$

$$-\frac{\rho}{r}\left[\frac{\partial}{\partial t}+U\,\frac{\partial}{\partial z}\right]\frac{\partial\Psi}{\partial r}=\frac{1}{r}\tau_{rz}^{(1)}+\frac{\partial}{\partial r}\,(\tau_{rz}^{(1)})+\frac{\partial}{\partial r}\,(\tau_{zz}^{(1)}), \tag{11}$$

while the continuity equation

$$\frac{1}{r}\,\frac{\partial}{\partial r}\,(rv^{(1)})+\frac{1}{r}\,\frac{\partial}{\partial z}\,(ru^{(1)})=0 \tag{12}$$

is automatically fulfilled.

To eliminate the pressure p contained in τ_{rr} and τ_{zz}, equation (10) is differentiated by z and (11) by r. By subtracting the resulting equations one obtains

Check

Check

$$\frac{\rho}{r}\left[\frac{\partial}{\partial t}+U\,\frac{\partial}{\partial z}\right]\mathrm{L}(\Psi)=\left[\frac{\partial^2}{\partial z^2}-\frac{\partial^2}{\partial r^2}-\frac{1}{r}\,\frac{\partial}{\partial r}+\frac{1}{r^2}\right]\tau_{rz}^{(1)} \tag{13}$$
$$+\frac{\partial^2}{\partial r\partial z}\,(\tau_{rr}^{(1)}-\tau_{zz}^{(1)})+\frac{1}{r}\,\frac{\partial}{\partial z}\,(\tau_{rr}^{(1)}-\tau_{\varphi\varphi}),$$

with L( ) as the linear differential operator

$$\mathrm{L}\equiv\frac{\partial^2}{\partial r^2}-\frac{1}{r}\,\frac{\partial}{\partial r}+\frac{\partial^2}{\partial z^2}\,. \tag{14}$$

Since in the context of the linear theory all disturbances must be proportional to η, the following ansatz is used:

Check

$$\Psi=UR\varphi(r/R)\eta(z,t),\ \text{i.e.:}\begin{cases}v^{(1)}=\mathrm{i}kRU\varphi\eta/r\\ u^{(1)}=-U\varphi'\eta/r\end{cases}, \tag{15}$$

$$\tau_{ij}^{(1)}=\left[-\rho U^2P(r/R)\delta_{ij}-\alpha_{ijkl}\rho\overline{u_k'u_l'}^{(0)}\right]\frac{\eta(z,t)}{R} \tag{16}$$

where[6] it has already been made use of the fact that for these quantities the differentiations to r, z, t p. 22

[6]Despite the curvilinear cylindrical coordinate system, Cartesian index notation with Einstein's summation convention is used here and elsewhere for the sake of clarity. It is summed over the indices k and l, as long as they occur twice; on the other hand, r, φ, z stand for free indexes that have already been allocated.

are[7]

$$\frac{\partial}{\partial r}(\,) = \frac{1}{R}\frac{\partial}{\partial(r/R)} = \frac{1}{R}(\,)', \quad \frac{\partial}{\partial z}(\,), \quad \frac{\partial}{\partial t}(\,) = -\mathrm{i}kc(\,) \tag{17}$$

In (16) the viscous frictional stresses were neglected compared to the turbulent pseudo-stresses and for the latter the existence of a connection of the form

$$\overline{u_i' u_j'}^{(1)}(r,z,t) = \alpha_{ijkl}(r/R)\,\overline{u_k' u_l'}^{(0)}\eta(z,t)/R \tag{18}$$

is provided. This implies the assumption that the apparent post-strain tensions are proportional to those in the undisturbed jet and proportional to the relative surface deformation η/R. As will be shown in sec. 1.4 this is compatible with a linear turbulence model like the RDT, but in a more general way, since the coefficient matrix α_{ijkl} allows the transfer of the fluctuation velocities from one coordinate direction to another. Check

The magnitude occurring in (16)

$$P(r/R) = \frac{p^{(1)}}{\rho U^2 \eta/R} \tag{19}$$

corresponds to a pressure coefficient. Substituting (15) and (16) into (13) yields an Orr-Sommerfeld equation in the form Check

$$(1-c^+)\left(\varphi'' - \frac{R}{r}\varphi'\xi^2\varphi\right) = T_{kl}\left(-\frac{\mathrm{i}r}{\xi R}\left[\left(\xi^2 - \frac{R^2}{r^2}\right)\alpha_{rzkl} + \frac{R}{r}\alpha'_{rzkl} + \alpha''_{rzkl}\right]\right. \tag{20}$$
$$\left. + \frac{r}{R}\left(\alpha'_{zzkl} - \alpha'_{rrkl}\right) + \alpha_{\varphi\varphi kl}\right),$$

where the dimensionless wavenumber and phase velocity p. 23

$$\xi = kR, \quad c^+ = c/U \tag{21}$$

and the constant tensor of the related double correlations characterizing the homogeneous turbulence in the undeformed jet Check

$$T_{kl} = \overline{u_k' u_l'}^{(0)}/U^2 \tag{22}$$

[7]Of course, the dash on u' still symbolizes the fluctuation size and should not be confused with the derivative with respect to r/R.

were introduced.

Since it does not depend on numerically exact results, but rather on the principal effect of turbulence on the jet breakup, to simplify the Orr-Sommerfeld Equation (20) as much as possible, independent of the specific proposition of a turbulence model: Check

First, it should be noted that reasonable solutions also exist for α_{zzkl}, α_{rrkl} = const., i.e, when the assumption is made that the turbulent normal stresses $\rho\overline{u_z'^2}^{(1)}$, $\rho\overline{u_r'^2}^{(1)}$ are constant over the jet cross section. For α_{rzkl} this is not possible because on the right side of (20) there is an r odd term Check

$$-\frac{\mathrm{i}}{\xi}(\xi^2 - R^2/r^2)\frac{r}{R}\alpha_{rzkl}T_{kl}$$

that would arise, which is impossible for symmetry reasons. The simplest approach for the coefficients α_{rzkl} (hence for the shear stress $\tau_{rz}^{(1)}$) is therefore a linear one in r.

On the right side of (20) there will still be $(\alpha_{\varphi\varphi kl} - \alpha_{rrkl})T_{kl}$. For reasons of balance, however, the undeformed jet is valid Check

$$\overline{u_r'^2}^{(0)} = \overline{u_\varphi'^2}^{(0)}, \quad \text{i.e.:} \quad T_{rr} = T_{\varphi\varphi}. \tag{23}$$

With a constant strain throughout the jet cross section, the fluctuation rates in the r and φ directions are alike, so that

$$(\alpha_{\varphi\varphi kl} - \alpha_{rrkl})T_{kl} \approx 0 \tag{24}$$

is a good approximation at least on average across the jet cross-section. With the mentioned simplifications, the Orr-Sommerfeld equation (20) is

$$(1 - c^+)\left(\varphi'' - \frac{R}{r}\varphi'\xi^2\varphi\right) = -\frac{\mathrm{i}r}{\xi R}\left[\left(\xi^2 - \frac{R^2}{r^2}\right)\alpha_{rzkl} + \frac{R}{r}\alpha'_{rzkl}\right]T_{kl}. \tag{25}$$

In this approximation remains on the right side, in a laminar case the effect of viscous frictional p. 24
stresses

$$-\frac{\mathrm{i}R^2}{\xi\mathrm{Re}}\,\mathrm{L}^2(\varphi) \quad \text{with} \quad \mathrm{Re} = \frac{UR}{\nu} \tag{26}$$

describes only the term left, resulting from the apparent stress $\tau_{rz}^{(1)}$, which was assumed to be linear in r as in a stratified flow. Check

1.3 Boundary conditions

The boundary conditions under which (25) is to be solved are the kinematic boundary condition and the condition of the local stress equilibrium on the surface to the frictionless surrounding medium.

The kinematic boundary condition at the edge of the jet[8]

$$\eta_t + u\,\eta_z = v \quad \text{at} \quad r = r_\mathrm{s} \tag{27}$$

returns when considering only the linear terms of the disturbances

$$v^{(1)} = \frac{1}{r}\frac{\partial \Psi}{\partial z} = \mathrm{i}k(U-c)\eta \quad \text{at} \quad r = R \tag{28}$$

or also with (15)

$$\varphi(1) = 1 - c^+. \tag{29}$$

The condition of the equilibrium of forces at the free surface demands

$$\tau_{ji} n_j = \hat{\tau}_{ji} n_j - \sigma\left(\frac{1}{R_1} + \frac{1}{R_2}\right) n_i. \tag{30}$$

For the sake of clarity, the effect of the ambient medium should first be neglected here, although, of course, in turbulent jets with their high velocities, this might be important. However, a subsequent extension to this effect is easily possible. This means

Check

$$\hat{\tau}_{ji} = \text{const} = -p_0 \delta_{ji},$$

and one obtains from (30) the two component equations

p. 25

$$\tau_{rr} n_r + \tau_{zr} n_z = -\left[p_0 + \sigma\left(\frac{1}{R_1} + \frac{1}{R_2}\right)\right] n_r, \tag{31}$$

$$\tau_{rz} n_r + \tau_{zz} n_z = -\left[p_0 + \sigma\left(\frac{1}{R_1} + \frac{1}{R_2}\right)\right] n_z, \tag{32}$$

[8]The indices on η stand for the derivatives according to the corresponding coordinates.

wherein the relationship between jet deformation and major radii of curvature is[9]

$$\frac{1}{R_1} + \frac{1}{R_2} = (1+\eta_z^2)^{-1/2}\left[\frac{1}{R+\eta} - \frac{\eta_{zz}}{1+\eta_z^2}\right]. \tag{33}$$

Under the use of

$$n_z/n_r = -n_z \tag{34}$$

and

$$\tau_{rr} = -p - \rho\overline{u_r'^2} = \tau_{zz} + \rho(\overline{u_z'^2} - \overline{u_r'^2}) \tag{35}$$

the system of equations (31) and (32) can be solved for τ_{zz} and $\tau_{rz} = \tau_{zr}$:

$$\tau_{zz}(r=r_\mathrm{s}) = -p_0 - \sigma\left(\frac{1}{R_1} + \frac{1}{R_2}\right) - \frac{1}{1-\eta_z^2}\rho(\overline{u_z'^2} - \overline{u_r'^2}), \tag{36}$$

$$\tau_{rz}(r=r_\mathrm{s}) = -\frac{\eta_z}{1-\eta_z^2}\rho(\overline{u_z'^2} - \overline{u_r'^2}). \tag{37}$$

By linearizing and highlighting the base solution, two equations arise, which the disturbances of the stress tensor at the jet edge $r = R$ must satisfy for equilibrium reasons:

$$\tau_{zz}(r=R) = \frac{\sigma}{R^2}(\eta + R^2\eta_{zz}) - \rho(\overline{u_z'^2} - \overline{u_r'^2}), \tag{38}$$

$$\tau_{rz}(r=R) = -\eta_z\rho(\overline{u_z'^2} - \overline{u_r'^2}). \tag{39}$$

If we now insert (16), we obtain the conditions for the coefficients α_{ijkl} at the jet boundary: p. 26

$$-(P(1) + \alpha_{zzkl}T_{kl}) = \frac{1}{\mathrm{We}}(1-\xi^2) - (\alpha_{zzkl} - \alpha_{rrkl})T_k l, \tag{40}$$

$$\alpha_{rzkl}(1)T_{kl} = \mathrm{i}\xi(T_{zz} - T_{rr}), \tag{41}$$

where the derivatives of η were calculated using (5) and the Weber number

$$\mathrm{We} = \frac{\rho U^2 R}{\sigma} \tag{42}$$

was introduced. For example, the pressure coefficient $P(r/R)$ still contained in (40) can be eliminated Check

[9] See, e.g., Yuen [Yue68] and Torpey [Tor89].

using (11). By substituting (15), (16), and (19) into this equation, one obtains the relationship

$$P + \alpha_{zzkl} T_{kl} = (1 - c^+) \frac{R}{r} \varphi' + \frac{\mathrm{i} R}{\xi r} \left[\frac{r}{R} \alpha_{rzkl} \right]' T_{kl}, \tag{43}$$

which is inserted into the normal-stress boundary condition (40), leads to the equation:

$$(1 - c^+) \varphi'(1) = -\frac{1}{\mathrm{We}} (1 - \xi^2) + \left[\alpha_{zzkl} - \alpha_{rrkl} - \frac{\mathrm{i}}{\xi} \left[\frac{r}{R} \alpha_{rzkl} \right]' \right]_{r=R} T_{kl}. \tag{44}$$

With the already established assumption of a linear distribution of α_{rzkl} over r, we obtain from (41) the distribution function of $\overline{u'_r u'_z}^{(1)}/U^2$

$$\alpha_{rzkl}(r/R) T_{kl} = \mathrm{i}\xi \frac{r}{R} (T_{zz} - T_{rr}), \tag{45}$$

which shows that for the important special case of isotropic turbulence in the undeformed jet the apparent stress $\tau_{rz}^{(1)} = -\rho \overline{u'_r u'_z}^{(1)}$ vanishes identically. The normal-stress boundary condition (44) is simplified to (45)

$$(1 - c^+) \varphi'(1) = -\frac{1}{\mathrm{We}} (1 - \xi^2) + (\alpha_{zzkl} - \alpha_{rrkl}) T_{kl} + 2(T_{zz} - T_{rr}), \tag{46}$$

and becomes the Orr-Sommerfeld equation (25)

$$(1 - c^+) \left(\varphi'' - \frac{R}{r} \varphi' - \xi^2 \varphi \right) = \xi^2 \frac{r^2}{R^2} (T_{zz} - T_{rr}). \tag{47}$$

As turbulence parameters two quantities appear in (46) and (47). The first p. 27

$$T_{\mathrm{N}} = (\alpha_{zzkl} - \alpha_{rrkl}) T_{kl} = (\overline{u'^2_z}^{(1)} - \overline{u'^2_r}^{(1)})/U^2 \tag{48}$$

is called in the further normal stress coefficient and describes the change of the turbulent normal stress difference due to a surface deformation. The second

$$T_{\mathrm{A}} = (T_{zz} - T_{rr}) = (\overline{u'^2_z}^{(0)} - \overline{u'^2_r}^{(0)})/U^2 \tag{49}$$

describes the same normal stress difference in the undeformed jet and is thus an anisotropy index.

Substituting this metric in (46) and (47) yields the Orr-Sommerfeld equation

$$(1-c^+)\left(\varphi'' - \frac{R}{r}\varphi' - \xi^2\varphi\right) = \xi^2\frac{r^2}{R^2}T_\mathrm{A} \tag{50}$$

and as a normal stress boundary condition

$$(1-c^+)\varphi'(1) = -\frac{1}{\mathrm{We}}(1-\xi^2) + T_\mathrm{N} + 2T_\mathrm{A}. \tag{51}$$

(50) is under the kinematic boundary condition (29) and the regularity condition resulting from (15)

$$\varphi(0) = \varphi'(0) = 0 \tag{52}$$

depending on ξ and c^+. Inserting $\varphi'(1)$ from this solution in (51) then yields a determination equation for c^+ whose imaginary part according to (5) is a measure of the magnification of perturbations. Check

This calculation can be done by specifying T_N and T_A, without any statements about the coefficients α_{ijkl} being necessary. The solution of the linear differential equation (50), already mentioned in the regularity conditions (52), is

$$\varphi = C\frac{r}{R}\,\mathrm{I}_1\left(\xi\frac{r}{R}\right) - \frac{T_\mathrm{A}}{1-c^+}\left[\frac{r}{R}\right]^2, \tag{53}$$

with $\mathrm{I}_\nu(x)$ as the modified Bessel function of the first kind, ν-th order, for which the derivative rule

$$\frac{\mathrm{d}}{\mathrm{d}x}\left[x^\nu\,\mathrm{I}_\nu(x)\right] = x^\nu\,\mathrm{I}_{\nu-1}(x) \tag{54}$$

applies.[10] The second term in (53) corresponds to the particular solution of the inhomogeneous differential equation for anisotropic turbulence ($T_\mathrm{A} \neq 0$). The still free constant C of the homogeneous solution fraction follows from the kinematic boundary condition (29) p. 28

$$C = \frac{1}{\mathrm{I}_1(\xi)}\left[1 - c^+ + \frac{T_\mathrm{A}}{1-c^+}\right], \tag{55}$$

so that the adapted solution for the stream function is ($\Psi = UR\varphi\eta$)

$$\varphi(r/R) = \frac{r}{R}\frac{\mathrm{I}_1(\xi r/R)}{\mathrm{I}_1(\xi)}\left[1 - c^+ + \frac{T_\mathrm{A}}{1-c^+}\right] - \frac{T_\mathrm{A}}{1-c^+}\left[\frac{r}{R}\right]^2. \tag{56}$$

[10] See [Wat44].

The derivative $\varphi'(r/R)$ required for the evaluation of the normal stress boundary condition (51), which according to (15) is also simultaneously proportional to the disturbance velocity in the axis direction ($u^{(1)} = -U\varphi'\eta/r$), calculated using (54)

$$\varphi'(r/R) = (1-c^+)\frac{r}{R}\frac{\xi\,\mathrm{I}_0(\xi r/R)}{\mathrm{I}_1(\xi)} + \frac{T_\mathrm{A}}{1-c^+}\frac{r}{R}\left[\frac{\xi\,\mathrm{I}_0(\xi r/R)}{\mathrm{I}_1(\xi)} - 2\right], \tag{57}$$

that is used in (51) yields the sought-after equation for the complex phase velocity c^+: Check

$$(1-c^+)^2\frac{\xi\,\mathrm{I}_0(\xi)}{\mathrm{I}_1(\xi)} = -\frac{1}{\mathrm{We}}(1-\xi^2) + T_\mathrm{N} + T_\mathrm{A}\left[4 - \frac{\xi\,\mathrm{I}_0(\xi)}{\mathrm{I}_1(\xi)}\right]. \tag{58}$$

Because of the neglect of the aerodynamic effect of the environment, (58) is independent of U in terms of the phase velocity *c relative to the baseline*. The jet "only" notices its speed via the relative movement to the atmosphere. In (58) this becomes clear when multiplying by the Weber number:

$$\frac{(U-c)^2}{\sigma/(\rho R)}\frac{\xi\,\mathrm{I}_0(\xi)}{\mathrm{I}_1(\xi)} = -(1-\xi^2) + S. \tag{59}$$

In doing so, the parameter automatically results Check

$$\begin{aligned} S(\xi) &= \mathrm{We}T_\mathrm{N} + \mathrm{We}T_\mathrm{A}\left[4 - \frac{\xi\,\mathrm{I}_0(\xi)}{\mathrm{I}_1(\xi)}\right] \\ &= \frac{\overline{u_z'^2}^{(1)} - \overline{u_r'^2}^{(1)}}{\sigma/(\rho R)} + \frac{\overline{u_z'^2}^{(0)} - \overline{u_r'^2}^{(0)}}{\sigma/(\rho R)}\left[4 - \frac{\xi\,\mathrm{I}_0(\xi)}{\mathrm{I}_1(\xi)}\right]. \end{aligned} \tag{60}$$

In (59) and (60), as already mentioned in the chapter 1, section 2, the typical velocity $[\sigma/(\rho R)]^{1/2}$ Check has assumed the role of the reference velocity.

The solution of (59) is:[11]

$$\frac{U-c}{\sqrt{\sigma/(\rho R)}} = \pm\sqrt{\frac{\mathrm{I}_1(\xi)}{\xi\,\mathrm{I}_0(\xi)}(\xi^2 - 1 + S)}. \tag{61}$$

[11] For $S = 0$ (that is, without turbulence), this result is absolutely equivalent to Rayleigh's classic solution [Ray78].

For $\xi^2 > 1 - S$, c is real and the waves grow at differential speed Check

$$|c - U| = \sqrt{\frac{\sigma R}{\rho}} \sqrt{\frac{\mathrm{I}_1(\xi)}{\xi\, \mathrm{I}_0(\xi)} (\xi^2 - 1 + S)} \quad (\xi^2 > 1 - S) \tag{62}$$

relative to the base flow. For $\xi^2 > 1 - S$, c is complex: the real part is U and the imaginary part

$$\mathrm{Im}(c) = \pm \sqrt{\frac{\sigma R}{\rho}} \sqrt{\frac{\mathrm{I}_1(\xi)}{\xi\, \mathrm{I}_0(\xi)} (1 - \xi^2 - S)} \quad (\xi^2 < 1 - S). \tag{63}$$

As can be seen from (5), $\mathrm{Im}(c) > 0$ means temporal growth of the waves, i.e., instability. It is customary to specify the rate of growth over time in a reference system fixed with the base flow[12]

$$\beta = \mathrm{i}k(U - c), \tag{64}$$

but in the case of spatially periodic waves considered here (k, ξ real) is identical to the growth rate at the fixed location z. If one uses as a reference time for β the typical time

$$\tau_{\mathrm{ref}} = (\rho R^3/\sigma)^{1/2}, \tag{65}$$

we get $\beta^* = \beta\tau_{\mathrm{ref}}$ for the dimensionless growth rate p. 30

$$\mathrm{Re}(\beta^*) = \pm\xi \mathrm{Re} \left\{ \sqrt{\frac{\mathrm{I}_1(\xi)}{\xi\, \mathrm{I}_0(\xi)} (1 - \xi^2 - S)} \right\}. \tag{66}$$

Thus, the sign of S determines whether the turbulence characterized by S is stabilizing (S positive) or destabilizing (S negative). To answer this question, of course, a turbulence model must be used; however, the following considerations are possible in advance:

Considering the wavenumber range $\xi < 1$, which is unstable in the laminar case, the estimate is (with a maximum error of +12% at $\xi = 1$)

$$\frac{\mathrm{I}_1(\xi)}{\xi\, \mathrm{I}_0(\xi)} \approx 2 \quad (|\xi| \leq 1), \tag{67}$$

[12] See Sterling and Sleicher [SS75].

which applied to (60) leads to Check

$$S(\xi) \approx \mathrm{We}(T_\mathrm{N} + 2T_\mathrm{A}). \tag{68}$$

For $T_\mathrm{N} + 2T_\mathrm{A} > 0$ stabilization by turbulence occurs. In the isotropic case, $T_\mathrm{A} = 0$, and T_N alone determines this question. The discussion in connection with fig. 1.3 (chapter 1, section 4), however, is to directly deduce that this quantity must be positive. It has been found that after a contraction (i.e. $\eta < 0$) $\overline{u_r'^2} > \overline{u_z'^2}$, and vice versa, after a cross-section extension (i.e. $\eta > 0$), $\overline{u_z'^2} > \overline{u_r'^2}$. According to (48) T_N is proportional to the η change of $\overline{u_z'^2} - \overline{u_r'^2}$, so definitely positive. The anisotropy parameter T_A according to (49), on the other hand, can be positive or negative, depending on which square mean value dominates in the undeformed jet. For $\overline{u_z'^2} - \overline{u_r'^2} > 0$, which is on average true for a pipe flow [13], it would be positive and then also stabilizing. Directly behind a nozzle, however, according to the discussion above, $T_\mathrm{A} < 0$ and thus could have a destabilizing effect if this anisotropy does not affect T_N.

1.4 Turbulence model

The task of the turbulence model is to determine the normal stress index T_N according to (48), p. 31
which together with the anisotropy index T_A to be specified according to (49) the size S in (66) specifies so that the fueling rates β^* can be determined from this equation. For this purpose, the two coefficient matrices α_{zzkl} and α_{rrkl} are to be calculated, which, as the following analysis shows, can be represented by assuming homogeneous-isotropic turbulence from two scalar quantities.

As already mentioned, the RDT is used for this[14]. The essential requirements for the applicability of this theory have already been mentioned in chapter 1, section 4. The extent to which they are fulfilled cannot be discussed independently of specific flow conditions such as nozzle shape, nozzle inflow, Reynolds number, etc. In connection with the experimental part of this work, the turbulence structures that are generated by a screen are of particular interest. As is well known, a few mesh sizes downstream behind such a turbulence screen, the turbulence is with good approximation homogeneous and approximately isotropic.[15] By stretching the liquid such as e.g. occurs in the nozzle, this isotropy is destroyed, but the anisotropies resonate due to the effect of turbulent pressure Check
forces[16] downstream again, and isotropic turbulence can be expected again at a sufficient nozzle spacing. The condition of the viscous dissipation negligible during the deformation cannot be fulfilled in the case of the jet. The deformation process, which finally leads to pinching off of the

[13] See Schlichting [Sch87].
[14] See Batchelor and Proudman [BP54].
[15] See Mohamed and Larue [ML90] and Reynolds and Tucker [RT75].
[16] See Batchelor [Bat53, pp. 87–88].

drops, takes so much time that the jet liquid has traveled a distance in the meantime, over which the turbulence could dissipate. However, as shown below, the typical length L_D of the dissipation process is much larger than the wavelength λ of the surface waves, so that the characteristics of the turbulence as a slowly changing element only flow into the solution parametrically. The application of the RDT is then based on the assumption that the decaying turbulence — described by $\overline{u_z'^2}^{(0)}(z)$ and an anisotropy parameter — continues to go into this theory, as is the case for a constant turbulence structure. This corresponds to a linear superposition of dissipation and deformation effects, as already suggested by Tucker and Reynolds [TR68]. Check

1.4.1 Estimation of the typical length of turbulent energy dissipation

The decay of the turbulence is estimated using the empirical relationship valid for a screen flow (mesh size M, wire diameter d)[17] p. 32

$$\frac{\overline{u'^2}}{U^2} = \mathrm{fcn}(UM/\nu, d/M) \cdot \left[\frac{z - z_0}{M}\right]^{-1}, \tag{69}$$

in which $z - z_0$ the screen distance corrected by a constant ($z_0/M \approx 10$) downstream and $\overline{u'^2}$ is a measure of the turbulent kinetic energy. One sets for the length scale Check

$$L_D = \frac{\overline{u'^2}}{U^2} \Bigg/ \frac{\mathrm{d}}{\mathrm{d}z}\left[\frac{\overline{u'^2}}{U^2}\right] = z - z_0, \tag{70}$$

the expression for the ratio L_d/λ from dissipation length to interference wavelength is obtained Check

$$L_D/\lambda = (z - z_0)/\lambda, \tag{71}$$

which becomes considerably larger than one for sufficiently large nozzle distances z.

1.4.2 Isotropic turbulence

Furthermore, the consideration should initially be limited to the case of isotropic turbulence before the rotationally symmetrical deformation. The turbulence model you are looking for can be given in explicit form for this important special case. The generalization to anisotropic turbulence is, however, easily possible, as will be shown below.

[17] See Batchelor [Bat53, p. 135], Mohamed and Larue [ML90] and Lewalle [Lew90].

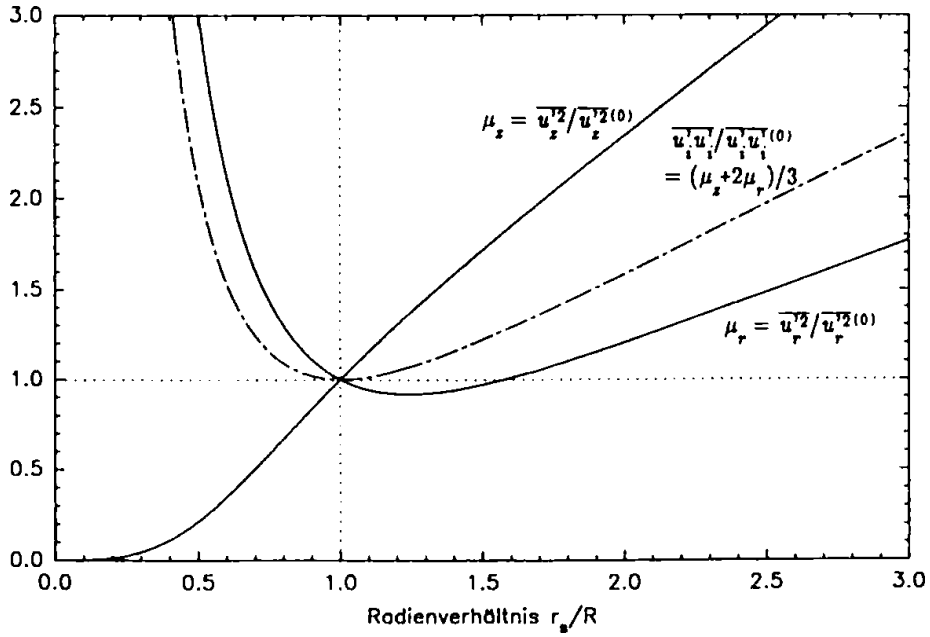

Figure 4: Results of Rapid Distortion Theory in isotropic turbulence. Translator's note: *Radienverhältnis = radius ratio*.

Under the conditions mentioned, the changes in the turbulent normal stresses at least approximately satisfy the relationships resulting from the RDT

$$\mu_z = \overline{u_z'^2}/\overline{u_z'^2}^{(0)} = \frac{3}{4\alpha^2 c^2}\left[\frac{1+\alpha^2}{2\alpha}\ln\frac{1+\alpha}{1-\alpha} - 1\right] \tag{72}$$

$$\mu_r = \overline{u_r'^2}/\overline{u_r'^2}^{(0)} = \frac{3}{4}c + \frac{3}{4\alpha^2 c^2}\left[\frac{1}{2} - \frac{1-\alpha^2}{4\alpha}\ln\frac{1+\alpha}{1-\alpha}\right]$$

with

$$\alpha^2 = 1 - c^{-3} \tag{73}$$

and c as the axial direction elongation

$$c = \mathrm{d}z/\mathrm{d}z^{(0)}. \tag{74}$$

In (74) $\mathrm{d}z^{(0)}$ and $\mathrm{d}z$ are material line elements before and after the jet deformation, the ratio of which can be expressed by the jet radius. Under the simplifying assumption that the elongation is p. 33

constant over the jet cross-section, mass conservation is required

$$\mathrm{d}z^{(0)}\pi R^2 = \mathrm{d}z\pi r_\mathrm{s}^2, \tag{75}$$

so

$$c = \mathrm{d}z/\mathrm{d}z^{(0)} = \frac{R^2}{r_\mathrm{s}^2} = 1 - 2\eta/R + O(\eta/R)^2. \tag{76}$$

The nonlinear relationship between the turbulent normal stresses and the jet radius resulting from (72)–(76) is plotted in figure 4. For the linear perturbation calculation, his Taylor series expansion has to be calculated by $r_\mathrm{s}/R = 1$ or $\eta = 0$. The linear term of this development in η is

$$\begin{aligned} \mu_z &= 1 + \overline{u_z'^2}^{(1)} / \overline{u_z'^2}^{(0)} = 1 + \frac{8}{5}\eta/R + O(\eta/R)^2, \\ \mu_r &= 1 + \overline{u_r'^2}^{(1)} / \overline{u_r'^2}^{(0)} = 1 - \frac{4}{5}\eta/R + O(\eta/R)^2, \end{aligned} \tag{77}$$

so that the comparison with (18) p. 34

$$\alpha_{zzkl} = \frac{8}{5}\delta_{kz}\delta_{lz}, \quad \alpha_{rrkl} = -\frac{4}{5}\delta_{kr}\delta lr \quad \Rightarrow T_\mathrm{N} = \frac{12}{5}T_{zz} \tag{78}$$

supplies. According to this result, the changes in the components of the turbulent normal stresses proportional to the same normal stresses in the undeformed jet and proportional to the jet deformation η. Check

1.4.3 Anisotropic turbulence

Is the turbulence in the undeformed jet anisotropic, i.e. $T_{zz} \neq T_{rr}$, can still be assumed from (72). The stretch c must then be overlaid with an virtual stretch c_v that is just large enough to produce the existing anisotropy.[18] (Such pre-stretching — e.g. through a nozzle — is also one of the possible causes of anisotropy.) The determination equation for c_v arises from the following consideration: Using of (72) is $\overline{u_z'^2}^{(0)} = \mu_z(c_\mathrm{v})\overline{u_z'^2}^{(*)}$ and $\overline{u_r'^2}^{(0)} = \mu_r(c_\mathrm{v})\overline{u_r'^2}^{(*)}$, whereby the sizes $\overline{u_z'^2}^{(*)} = \overline{u_r'^2}^{(*)}$ Check

[18] This approach to the use of RDT even with anisotropic turbulence prior to the deformation was proposed by Reynolds and Tucker [RT75] and is adopted here.

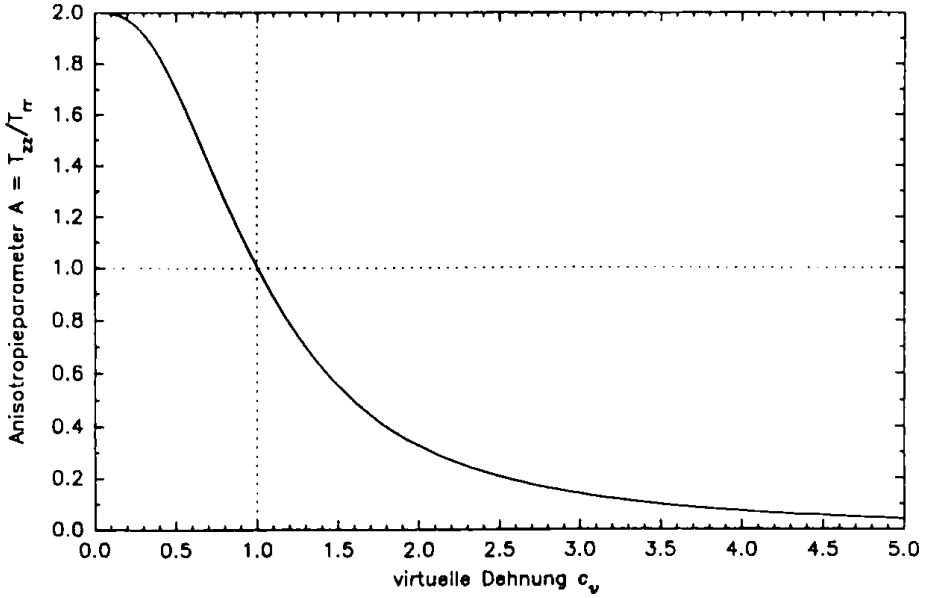

Figure 5: Relationship between the anisotropy of turbulence in the undeformed jet and the virtual strain c_v. Translator's note: *Anisotropieparameter* = *anisotropy parameter* and *virtuelle Dehnung* = *virtual stretch*.

correspond to an virtual isotropic reference state. This determines c_v from the condition Check

$$A := \frac{\overline{u_z'^2}^{(0)}}{\overline{u_r'^2}^{(0)}} = \frac{\mu_z(c_\mathrm{v})}{\mu_r(c_\mathrm{v})}, \quad \text{in which} \quad A = \frac{T_{zz}}{T_{rr}} \tag{79}$$

is used in the following as the second anisotropy parameter, which is connected to the key figure according to (49) via $T_\mathrm{A} = (1 - 1/A)T_{zz}$. The relationship given by (79) and (72) is plotted in figure 5. As you can see, A varies between the value 2 for $c_\mathrm{v} \to 0$ and 0 for $c_c \to \infty$. For a known value of A, the value of c_v can be read on the abscissa. Check

The total strain then corresponds to the product of the virtual and actual strain:

$$c_\mathrm{ges} = c_\mathrm{v} \cdot c. \tag{80}$$

The relationship between the physical strain c and the change in the turbulent fluctuation velocities is representative of the example of the component $\overline{u_z'^2}$. The easiest way to derive this is again using the reference variable $\overline{u_z'^2}^{(*)}$ in the virtual state $c = c_\mathrm{v} = 1$. Under the effect of the total Check p. 35

stretch $c \cdot c_\mathrm{v}$, $\overline{u_z'^2} = \mu_z(c_\mathrm{ges})\overline{u_z'^2}^{(*)}$ [19] Because of the decomposition $\overline{u_z'^2} = \overline{u_z'^2}^{(1)} + \overline{u_z'^2}^{(0)}$ follows from this

$$\frac{\overline{u_z'^2}^{(1)}}{\overline{u_z'^2}^{(0)}} = \frac{\mu_z(c_\mathrm{ges})}{\mu_z(c_\mathrm{v})} - 1, \tag{81}$$

where because of (76) and (80)

$$c_\mathrm{ges} = c_\mathrm{v} \cdot (1 - 2\eta/R + O(\eta/R)^2) \tag{82}$$

applies. To calculate the Taylor series of (81) for small η, μ_z does not have to be developed by $c = 1$ as in the case of isotropic turbulence, but by $c = c_\mathrm{v}$:

$$\begin{aligned}\mu_z(c_\mathrm{ges}) &= \mu_z(c_\mathrm{v}) + \mu_z'(c_\mathrm{v})\,\frac{\mathrm{d}c_\mathrm{ges}}{\mathrm{d}\eta}\,\eta + O(\eta/R)^2 \\ &= \mu_z(c_\mathrm{v}) - 2\mu_z'(c_\mathrm{v})c_\mathrm{v}\eta/R + O(\eta/R)^2.\end{aligned} \tag{83}$$

By inserting in (81) one finally gains neglecting at least quadratic terms in η/R p. 36

$$\frac{\overline{u_z'^2}^{(1)}}{\overline{u_z'^2}^{(0)}} = -2\frac{\mu_z'(c_\mathrm{v})}{\mu_z(c_\mathrm{v})}c_\mathrm{v}\frac{\eta}{R}, \quad \frac{\overline{u_r'^2}^{(1)}}{\overline{u_r'^2}^{(0)}} = -2\frac{\mu_r'(c_\mathrm{v})}{\mu_r(c_\mathrm{v})}c_\mathrm{v}\frac{\eta}{R}, \tag{84}$$

whereby the r component was treated quite analogously.

So the generalization of (78) to the case of anisotropic turbulence in the undeformed jet is

$$\alpha_{zzkl} = \alpha_z(c_\mathrm{v})\delta_{kz}\delta_{lz}, \quad \alpha_{rrkl} = \alpha_r(c_\mathrm{v})\delta_{kr}\delta_{lr}, \tag{85}$$

with

$$\alpha_z(c_\mathrm{v}) = -2\frac{\mu_z'(c_\mathrm{v})}{\mu_z(c_\mathrm{v})}c_\mathrm{v}, \quad \alpha_r(c_\mathrm{v}) = -2\frac{\mu_r'(c_\mathrm{v})}{\mu_r(c_\mathrm{v})}c_\mathrm{v}. \tag{86}$$

[19] Translator's note: The starred term was missing the z subscript in the original.

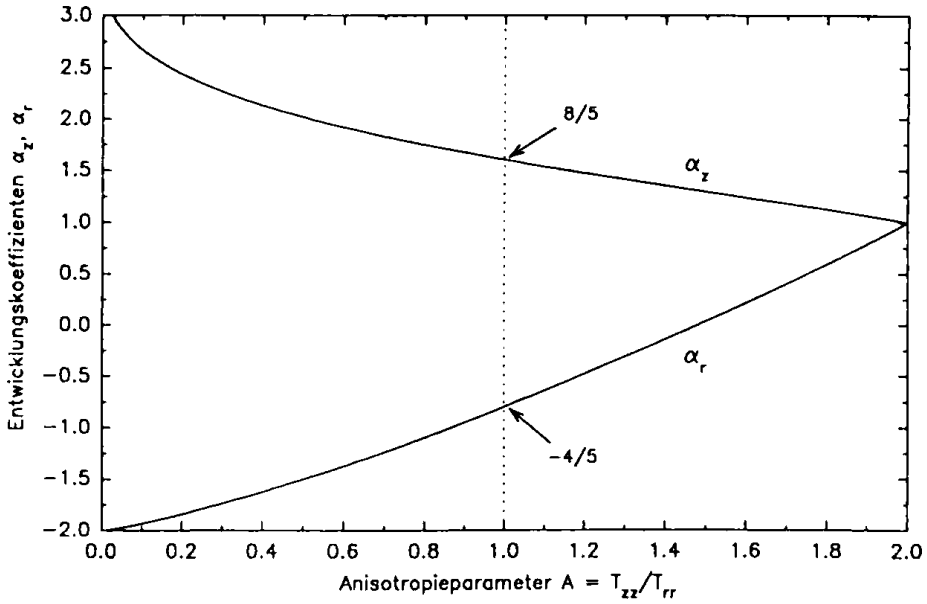

Figure 6: Development coefficients of the turbulent normal stresses. Translator's note: *Entwicklungskoeffizienten* = *development coefficients* and *Anisotropieparameter* = *anisotropy parameter*.

The derivatives of μ_z and μ_r to c that occur in it are according to (72)

$$\mu_z' = -\frac{2}{c}\mu_z + \frac{9}{8\alpha^4 c^5}\left[\frac{2\alpha^2 - 3(1+\alpha^2)}{2\alpha}\ln\frac{1+\alpha}{1-\alpha} + \frac{1+\alpha^2}{1-\alpha^2} + 2\right],$$
$$\mu_r' = \frac{9}{4} - \frac{2}{c}\mu_r + \frac{9}{8\alpha^4 c^5}\left[\frac{2\alpha^2 + 3(1-\alpha^2)}{4\alpha}\ln\frac{1+\alpha}{1-\alpha} - \frac{3}{2}\right], \tag{87}$$

where $\alpha(c)$ is given by (73). With $c_\mathrm{v} = c_\mathrm{v}(A)$ from figure 5 (86) provides the relationship shown in figure 6 between the development coefficients α_z, α_r and the degree of anisotropy $A = T_{zz}/T_{rr}$. For the special case of isotropy, the numerical values $\alpha_z = 8/5$, $\alpha_r = -4/5$ are obtained again. The two turbulence indicators are calculated from this

$$T_N = (\alpha_z(A) - \alpha_r(A)/A)T_{zz},$$
$$T_A = (1 - 1/A)T_{zz}. \tag{88}$$

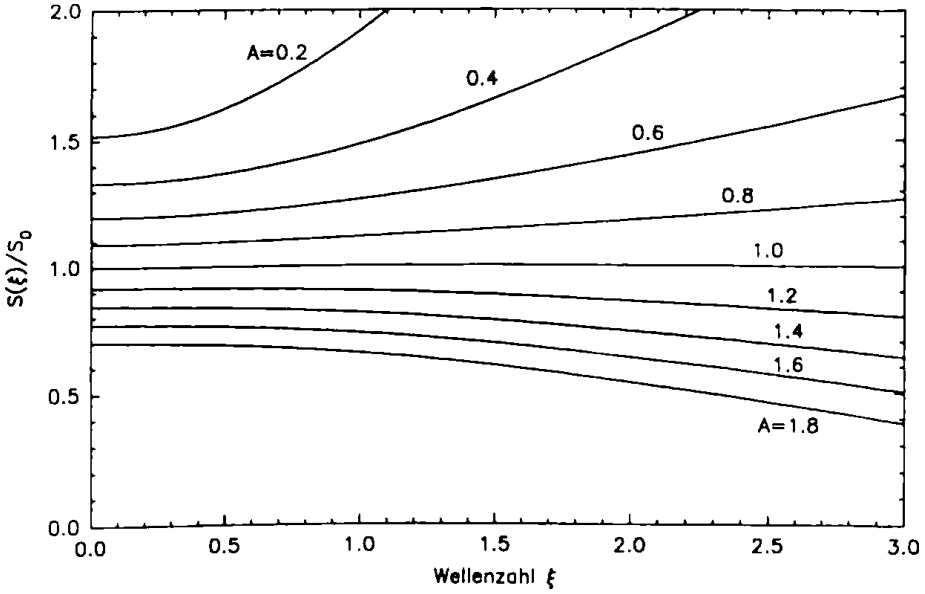

Figure 7: Turbulence parameter $S(\xi)/S_0$ according to (89) for different degrees of anisotropy A. Translator's note: *Wellenzahl* = *wavenumber*.

1.5 Calculation of the growth rates

Now the magnitude S can be specified in the determination equation (66) for the growth rate β^*. Check p. 37
The expression is obtained from (60) and (88)

$$S(\xi) = S_0 \frac{5}{12} \left\{ \alpha_z - \frac{\alpha_r}{A} + \frac{A-1}{a} \left[4 - \frac{\xi \, \mathrm{I}_0(\xi)}{\mathrm{I}_1(\xi)} \right] \right\}, \tag{89}$$

its pre-factor

$$S_0 = \frac{12}{5} \mathrm{We} T_{zz} = \frac{12}{5} \frac{\overline{u_z'^2}^{(0)}}{\sigma/(\rho R)} \tag{90}$$

is proportional to the ratio of the turbulent kinetic energy per unit of jet length to surface energy (see chapter 1, section 1.2). The pre-factor 12/5 results from the RDT and is chosen so that $S(\xi)/S_0$ becomes one for isotropic turbulence. The course of $S(\xi)/S_0$ over ξ can be seen for different degrees of anisotropy A in figure 7. It turns out that — insofar as the derived result of the RDT is also p. 38
reliable for anisotropic turbulence — the parameter S is positive in the whole relevant wave part. (Negative values only occur for $T_{zz} \gg T_{rr}$ and $\xi \gg 1$.) The effect of the turbulence is therefore always stabilizing!

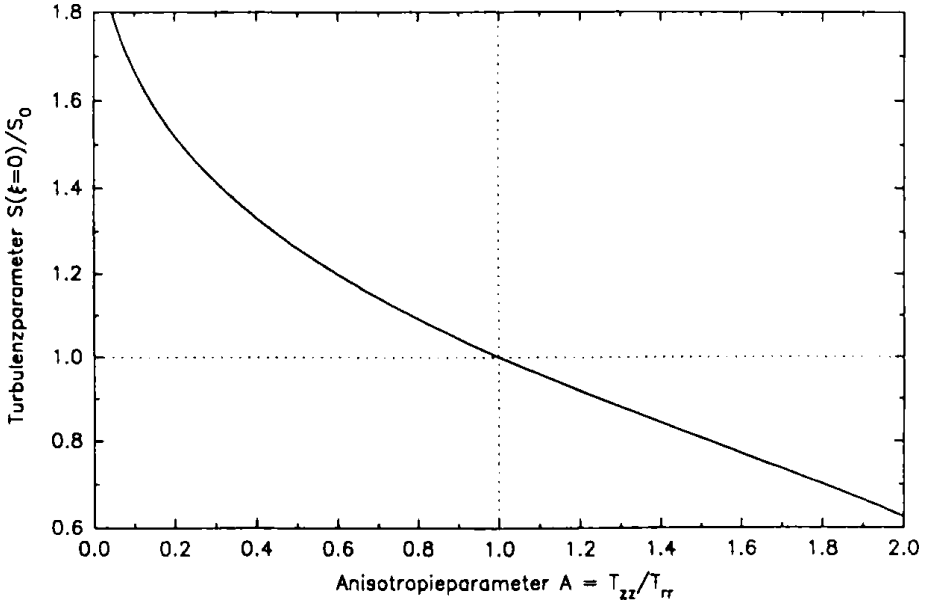

Figure 8: Turbulence parameter $S(\xi = 0)/S_0$. Translator's note: *Turbulenzparameter* = *turbulence parameter* and *Anisotropieparameter* = *anisotropy parameter*.

For positive S one excludes (66) such that within the unstable wavenumber range the restriction $|\xi| < 1$, which must be assumed for the simplification (67), is fulfilled. Within this approximation you get

$$S \approx S(\xi = 0) = S_0 \frac{5}{12} \left[\alpha_z - \frac{\alpha_r}{A} + 2\frac{A-1}{A} \right], \tag{91}$$

So just the ordinate values of the curves in figure 7, which are plotted in figure 8 above the anisotropy parameter A.

The determination equation (66) for the rate of increase is simplified accordingly Check

$$\mathrm{Re}(\beta^*) = \pm\xi \mathrm{Re}\left[\sqrt{\tfrac{1}{2}(1 - \xi^2 - S)} \right]. \tag{92}$$

As the following sec. 2 shows, this is also the result of a quasi-one-dimensional analysis, in p. 39 which all flow variables over the jet cross section are assumed to be constant.[20]

The courses from $\mathrm{Re}(\beta^*)$ according to (92) are shown in figure 9. $S \approx S(\xi = 0)$ according to figure 8 serves as a constant share parameter. The positive sign in (92) is decisive for the wave

[20] See Weber [Web19, p. 12].

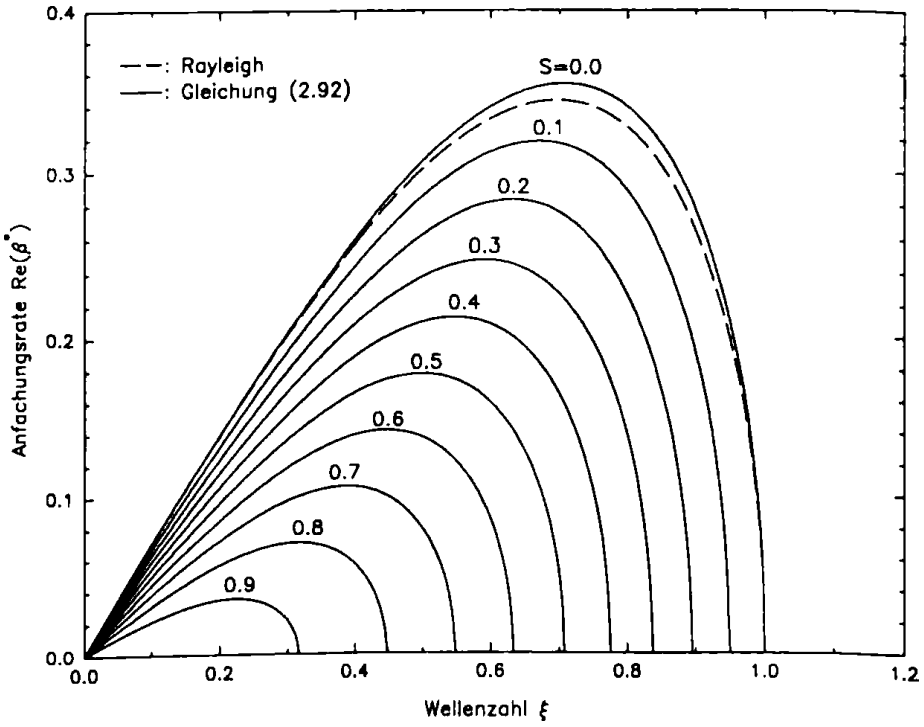

Figure 9: Growth rate curves for different values from S to (92), or dashed lines for $S = 0$ to (66). Translator's note: *Anfachungsrate* = *growth rate* and *Wellenzahl* = *wavenumber*.

growth, so that the diagram remains restricted to this part of the solution.

The dashed curve of the exact solution (66) for the laminar case corresponds to the Rayleigh solution. It differs only slightly from the result simplified with (67), which, as I said, is the solution of the one-dimensional one. Approximation is. The same applies to the curves with $S \neq 0$. This shows that even in the turbulent case within the unstable wavenumber range, a quasi-one-dimensional analysis of the problem provides sufficiently accurate results. Because of $\xi < 1$, i.e., $\lambda > 2\pi R$, the changes in the radial direction are very small and the assumptions of the current thread theory are fulfilled in a good approximation.

Together with the parameter S according to figure 8, figure 9 contains the central result of this work: Homogeneous turbulence stabilizes rotationally symmetrical surface waves. As a result of the normal stress effect, not only is the unstable wavenumber range restricted from $0 < \xi < 1$ to $0 < \xi < (1 - S)^{1/2}$, but also the maximum accumulation rates that occur with turbulence are significantly smaller. For $S = 1$, the growth of surface waves with total rotation is completely suppressed. p. 40 Check Check

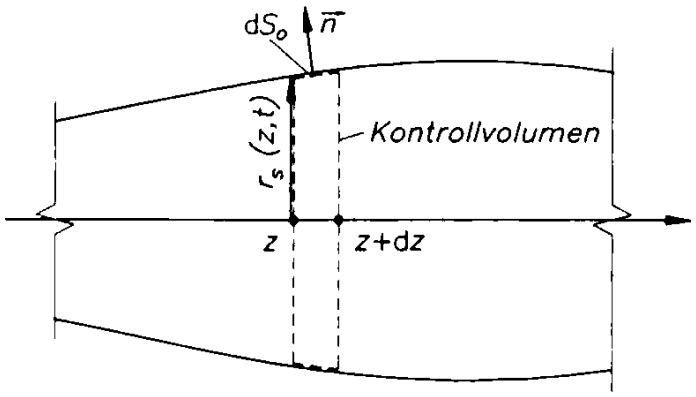

Figure 10: Control volume disk of the thickness dz. Translator's note: *Kontrollvolumen* = *control volume*.

For comparison with experiments, the result plotted in figure 9 must be expanded to take account of the environmental influence, which is done in section 4.1.1 (see fig. 4.1). The effect discussed here remains unaffected.

2 Quasi-one-dimensional view

2.1 Set of equations for finite deformations

As already noted in sec. 1.5, the unstable surface disturbances are so long-wave that they can be detected with a good approximation by a quasi-one-dimensional view. This one-dimensional theory is not only characterized by greater clarity, it is also the basis of the relatively inexpensive numerical solution of the non-linear problem, which is described in sec. 2.4. First of all, it is necessary to set up the differential equations describing the wave growth even with eventually large deformations. The basis is the stream filament theoretical conservation equations of mass and momentum [21], due to the control volume disk sketched in figure 10 with jet radius r_s and thickness dz. On the one hand, this creates the continuity equation p. 41 Check

$$\frac{\partial A}{\partial t} + \frac{\partial}{\partial z}(uA) = 0, \tag{93}$$

or with $A = \pi r_s^2$

$$2r_s \frac{\partial r_s}{\partial t} + \frac{\partial}{\partial z}(ur_s^2) = 0, \tag{94}$$

[21] SeeSpurk and Aksel [SA10, pp. 262 and 270].

and on the other hand the momentum equation in the form

$$\rho \left[\frac{\partial}{\partial t} (uA) + \frac{\partial}{\partial z} (u^2 A) \right] = \frac{\partial}{\partial z} (\tau_{zz} A) + \frac{\mathrm{d}F}{\mathrm{d}z}, \tag{95}$$

in the $\mathrm{d}F$ is the force in the z direction on the free surface $\mathrm{d}S_0$ of the jet disc under consideration. p. 42
This is calculated

$$\mathrm{d}F = \int \int_{\mathrm{d}S_0} t_z \, \mathrm{d}S = \int \int_{\mathrm{d}S_0} \tau_{zz} n_z \, \mathrm{d}S + \int \int_{\mathrm{d}S_0} \tau_{rz} n_r \, \mathrm{d}S. \tag{96}$$

The magnitudes $\left| n_z \, \mathrm{d}S \right|$ and $|n_r \, \mathrm{d}S|$ are the components of the surface element $\mathrm{d}S$ of the surface in Check
the axial or radial direction. The evaluation of the integrals therefore provides

$$\mathrm{d}F = -\tau_{zz} \, \mathrm{d}A + \tau_{rz}(r_\mathrm{s}) 2\pi r_\mathrm{s} \, \mathrm{d}z = \left[-\tau_{zz} \frac{\partial A}{\partial z} + \tau_{rz}(r_\mathrm{s}) 2\pi r_\mathrm{s} \right] \mathrm{d}z, \tag{97}$$

and the impulse theorem is after differentiation, use of the continuity equation (93) and division by A

$$\frac{\partial u}{\partial t} + u \frac{\partial u}{\partial z} = \frac{\partial}{\partial z} (\tau_{zz}/\rho) + \frac{2}{\rho r_\mathrm{s}} \tau_{rz}(r_\mathrm{s}). \tag{98}$$

Within the framework of the current thread theory, the part $r^{-1} \partial (r \tau_{rz}) / \partial r$ of the divergence of the tension tensor becomes the term $2\tau_{rz}(r_\mathrm{s})/r_\mathrm{s}$, which is equivalent to the assumption of a linear course from τ_{rz} over r, which was also made in sec. 1. The stress tensor components occurring in (98) are to be replaced by the equations (36) and (37) resulting from the equilibrium at the edge of the jet (in which η_z is to be replaced by $\partial r_\mathrm{s} / \partial z$) given, so that the impulse set the form

$$\frac{\partial u}{\partial t} + u \frac{\partial u}{\partial z} = \frac{\partial}{\partial z} \left[-\frac{\sigma}{\rho} \left(\frac{1}{R_1} + \frac{1}{R_2} \right) - \frac{\overline{u_z'^2} - \overline{u_r'^2}}{1 - (\partial r_\mathrm{s}/\partial z)^2} \right] - \frac{2}{r_\mathrm{s}} \frac{\overline{u_z'^2} - \overline{u_r'^2}}{1 - (\partial r_\mathrm{s}/\partial z)^2}. \tag{99}$$

assumes that the constancy of τ_{zz} over the jet cross-section was assumed. This equation can be expressed in the equivalent form

$$\frac{\partial u}{\partial t} + u \frac{\partial u}{\partial z} = -\frac{\sigma}{\rho} \frac{\partial}{\partial z} \left[\frac{1}{R_1} + \frac{1}{R_2} \right] - \frac{1}{r_\mathrm{s}^2} \frac{\partial}{\partial z} \left[\frac{\overline{u_z'^2} - \overline{u_r'^2}}{1 - (\partial r_\mathrm{s}/\partial z)^2} r_\mathrm{s}^2 \right], \tag{100}$$

which, if the turbulent normal stress difference $\overline{u_z'^2} - \overline{u_r'^2}$ is replaced by $(\tau_{rr} - \tau_{zz})/\rho$, becomes a form of the momentum equation that is also used in the calculation of thread spinning processes. Check

The impulse set (99) or (100) and the continuity equation (94) form the nonlinear equation set p. 43 for the two unknowns $r_s(z,t)$ and $u(z,t)$. The main radii of curvature are determined again from (33) and the turbulent normal stress difference from (72)[22].

The singularity occurring in (99) and (100) at $\partial r_s/\partial z = 1$, i.e. a surface slope of 45° results from the boundary condition of the equilibrium of forces on the free surface (31), (32). For $\partial r_s/\partial z = 1$ this requires $\tau_{rr} = \tau_{zz}$. If the surface deformation comes in areas of such large gradients, the limit of the one-dimensional theory has been reached. In particular, the assumption on which the expansion across the jet cross section is based, which is the basis in turbulence modeling, then loses its validity. The flow has such a pronounced spatial character that the liquid expansion can no longer be expressed solely via the jet radius.

For the numerical solution of the system of equations (94), (100) described in sec. 2.4, this singularity does not result in any significant restriction. Because of the long ripple of the unstable disturbances of interest, the surface slopes are so small up to very close to the breakup point that neglecting the term $(\partial r_s/\partial z)^2)$ in (100) has hardly any effect on the calculated contours, which is also confirmed by comparative calculations. Check

The stabilizing effect of turbulence can be explained using the momentum equation (100). However, let us first consider the laminar case: Without turbulence, within the framework of the one-dimensional approximation, the surface geometry defines a certain pressure distribution along the z axis via the capillary tension. The derivation of this pressure distribution according to z leads to an acceleration of the liquid[23]

$$\frac{\partial u}{\partial t} + u\,\frac{\partial u}{\partial z} = -\frac{\sigma}{\rho}\,\frac{\partial}{\partial z}\left[\frac{1}{R_1} + \frac{1}{R_2}\right] \quad \text{(laminar, frictionless)} \tag{101}$$

and is described by the first term on the right side of (100). For long-wave interference $1/R_1 + 1/R_2 \approx 1/r_s$, i.e. the maximum pressure is at points of minimum jet cross-section. This pressure distribution displaces the liquid axially from the trough and leads to the constriction of the jet.

The turbulent normal stress difference $\overline{u_z'^2} - \overline{u_r'^2}$ behaves differently, which occurs in the parentheses of the second term on the right-hand side of (100). This has a minimum in the wave valleys and consequently accelerates the liquid into constricted areas, which fills them up again and thus has a stabilizing effect.

[22] For anisotropic turbulence in the undeformed jet, the total elongation in (72) c must be replaced according to (80).
[23] See Torpey [Tor89].

2.2 Linear disturbance calculation

The stability investigation should initially remain restricted to the linear range of disturbances. p. 44

If one puts (4), (5) into the continuity equation (94) and only takes linear terms into account in η, one obtains the differential equation for the disturbance velocity

$$\frac{\partial u^{(1)}}{\partial z} = 2\mathrm{i}k(c-U)\eta/R \tag{102}$$

and from that Check

$$u^{(1)} = 2(c-U)\eta/R \tag{103}$$

The linearized form of (33) is

$$\frac{1}{R_1}+\frac{1}{R_2} = \frac{1}{R}\left(1-\frac{\eta}{R}\right) = \frac{1}{R}-\frac{1}{R^2}(1-\xi^2)\eta, \tag{104}$$

so that from the impulse set (99) after linearization and deletion of the base solution becomes Check

$$\frac{\partial u^{(1)}}{\partial t} + U\frac{\partial u^{(1)}}{\partial z} = \frac{\partial}{\partial z}\left[\frac{\sigma}{\rho R^2}(1-\xi^2)\eta - (\overline{u_z'^2}^{(0)} - \overline{u_r'^2}^{(1)})\right] - \frac{2}{R}\eta_z(\overline{u_z'^2}^{(1)} - \overline{u_r'^2}^{(0)}). \tag{105}$$

With $u^{(1)}$ from (103) and turbulence indicators T_N, T_A after (48) and (49) it follows

$$(1-c^+)^2 = -\frac{1}{2\mathrm{We}}(1-\xi^2) + T_\mathrm{A} + \frac{1}{2}T_\mathrm{N}, \tag{106}$$

which is identical to (58) if you simplify the Bessel functions according to (67). The resulting rate of increase is given by (92) and can be seen in figure 9.

2.3 Convective instability

So far it was assumed that the wave number k in the approach (5) for the surface waves $\eta(z,t)$ is p. 45 purely real. The waves thus described are spatially periodic and are fanned in time (or damped). However, the waves to be observed in the experiment are periodic in time with appropriate excitation, must disappear at the nozzle outlet for kinematic reasons and are spatially, i.e. fanned in the jet direction. In this section, therefore, the relationship between the previously calculated rate of

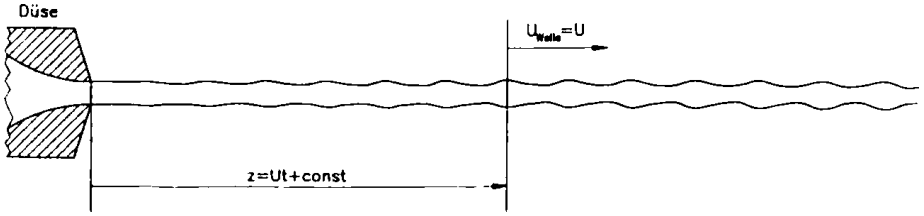

Figure 11: Model for converting temporary to convective instability. Translator's note: *Düse* = *nozzle* and *welle* = *wave*.

accretion and the convective rate will be examined.[24]

We do not take into account the influence of jet acceleration due to gravitation, although this secondary effect is of course inevitable in the experiment. In Appendix B, however, this aspect is dealt with and shown that an acceleration of the base flow on the convective wave growth has a stabilizing effect, which, however, is negligible with most large Froude numbers of turbulent jets.

For the laminar case, as is known, according to Gaster's theorem [Gas62], the spatial growth of unstable waves can be determined approximately directly from the temporal growth rate β. The model that leads to this conversion is as follows: Unstable waves have a phase velocity of U (see (61)), i.e. $t = z/U + \text{const}$ applies to a wave (figure 11). This immediately leads to $\eta \sim \exp(\beta t) \sim \exp(z\beta/U)$, which results in a spatial increase rate of β/U, requiring a large Weber number, because then the growth rates $\beta R/U = \beta^*/\mathrm{We}^{1/2}$ are small, and each wave train behaves as if the disturbances in z are periodic. Check Check

It is easy to show mathematically that this conversion is also possible in the turbulent case. For this, the approach for the deformation of the jet contour is used instead of (55): p. 46

$$\eta(z,t) = \eta_0 \mathrm{e}^{-\mathrm{i}\Omega t}\mathrm{e}^{\mathrm{i}kz} = \eta_0 \mathrm{e}^{-k_\mathrm{I}}\mathrm{e}^{\mathrm{i}(k_\mathrm{R} z - \Omega t)} \tag{107}$$

Spatial growth therefore requires a negative imaginary part of the complex wave number $k = k_\mathrm{R} + \mathrm{i}k_\mathrm{I}$. The only difference to the previous theory is the replacement (see (107) with (5))

$$c = \frac{\Omega}{k} \quad \text{or} \quad c^+ = \frac{\Omega R}{U}\frac{1}{\xi} \tag{108}$$

in (106):

$$\left[1 - \frac{\Omega R}{U}\frac{1}{\xi}\right]^2 = -\frac{1}{2\mathrm{We}}(1 - \xi^2 - S). \tag{109}$$

[24]On the subject of convective instability of the capillary jet see Keller, Rubinow, and Tu [KRT73], Leib and Goldstein [LG86a; LG86b], Lin and Lian [LL89; LL90], and Lin, Lian, and Creighton [LLC90].

After the introduction of the dimensionless temporal angular frequency Check

$$\Omega^+ = \frac{\Omega R}{U} \tag{110}$$

and the number

$$\chi = \frac{2\mathrm{We} + 1 - S}{2\mathrm{We}} \tag{111}$$

which is about one for large Weber numbers, where you obtain the relationship Check

$$\frac{1}{2\mathrm{We}}\xi^4 - \chi\xi^2 + 2\Omega^+\xi - \Omega^{+2} = 0. \tag{112}$$

Given Ω^+, We and S, this is a fourth order polynomial with real coefficients, the four solutions of which can be easily calculated using one of the standard polynomial root routines. For the non-turbulent case, (112) corresponds to the equation (A.11) given in Appendix A, which results from a development of the two-dimensional Weber's solution for small wavenumbers. (Because of the neglected viscosity, the terms dependent on Reynolds number are missing here.)

With the exception of the parameter range with small Weber numbers and large Ω^+ ($\mathrm{We} < 10$, $\Omega^+ \gg 1$), which is of no interest here, the following solutions are obtained: Two roots are purely real and have different signs. They are of the order of magnitude $(2\mathrm{We})^{1/2}$, which means that they are too short-wave in the assumed Weber numbers to be even roughly reproduced by the one-dimensional p. 47 theory.

The other two roots are complex conjugate in the range $0 < \Omega^+ < 1$. The real parts are approximately equal to Ω^+, while the imaginary parts differ only slightly from the value of the temporal increase according to (92):

$$\xi_\mathrm{I} \approx \beta^+ := \frac{\beta R}{U} = \beta^*/\mathrm{We}^{1/2}. \tag{113}$$

These two solutions are the ones that are obtained from the transformation according to figure 11. To prove this asymptotic behavior for large Weber numbers, first (112) is split into real and imaginary parts:

$$\frac{1}{2\mathrm{We}}(\xi_\mathrm{R}^4 - 6\xi_\mathrm{R}\xi_\mathrm{I}^2 + \xi_\mathrm{I}^4) - \chi(\xi_\mathrm{R}^2 - \xi_\mathrm{I}^2) + 2\Omega^+\xi_\mathrm{R} - \Omega^{+2} = 0, \tag{114}$$

$$\frac{1}{\mathrm{We}}(\xi_\mathrm{R}^3\xi_\mathrm{I} - \xi_\mathrm{R}\xi_\mathrm{I}^3) - \chi\xi_\mathrm{R}\xi_\mathrm{I} + \Omega^+\xi_\mathrm{I} = 0. \tag{115}$$

For unstable waves $\xi_I \neq 0$ 0 and the equation is obtained from (115)

$$\Omega^+ = \xi_R \left[\chi - \frac{1}{We} (\xi_R^2 - \xi_I^2) \right], \tag{116}$$

with which one can eliminate the parameter Ω^+ in (114). After a short interim calculation, the relationship emerges

$$\left[\frac{1}{2We} - \frac{1}{We^2} \xi_R^2 \right] \xi_I^4 + \left[\chi - \frac{1+2\chi}{We} \xi_R^2 + \frac{2}{We^2} \xi_R^4 \right] \xi_I^2 - \chi \frac{1-S}{2We} \xi_R^2 + \left[\frac{1}{2We} + \frac{1-S}{We^2} \right] \xi_R^4 - \frac{1}{We^2} \xi_R^6 = 0, \tag{117}$$

which, given ξ_R, is a quadratic equation for ξ_I^2. For ξ_I one obtains two real solutions of the same amount but different signs, which together with the real part ξ_R are the two conjugate complex solutions of (112). The solution of (117) is simplified for large Weber numbers

$$\xi_I We^{1/2} = \pm \xi_R \sqrt{\frac{1}{2}(1 - \xi_R^2 - S) + \frac{1}{4We} \left[3(1-S)\xi_R^2 - 2\xi_R^4 \right]} + O(We^{-2}). \tag{118}$$

This result is identical to (92) except for the term multiplied by $1/We$, if ξ is replaced by $\xi_R = \mathrm{Re}(\xi)$. p. 48
This would show the validity of (113) also for the turbulent case.

Finally, for large Weber numbers, the relationship (116) between the dimensionless frequency Ω^+ and the resulting wave number ξ_R can be specified explicitly. With (118) you get the relationship

$$\Omega^+ = \xi_R - \frac{1}{2We} \left[2\xi_R^3 - (1-S)\xi_R \right] + O(We^{-2}). \tag{119}$$

In figure 12 and figure 13 the courses of the spatial rate of increase — $\xi_I \cdot We^{1/2}$ over ξ_R according to (117) and the wave number ξ_R plotted over Ω^+ according to (116). Only the unstable solution with $\xi_I < 0$ was considered. As can be seen, the limit values for $We \to \infty$ are quickly reached with increasing Weber number. From $We \approx 50$, the differences between spatial and temporal rates of increase can no longer be represented. In figure 13, where for reasons of clarity only the course for $S = 0$ is shown, the same tendency results for $S \neq 0$, but with a restricted frequency or wavenumber range (see figure 9). Check

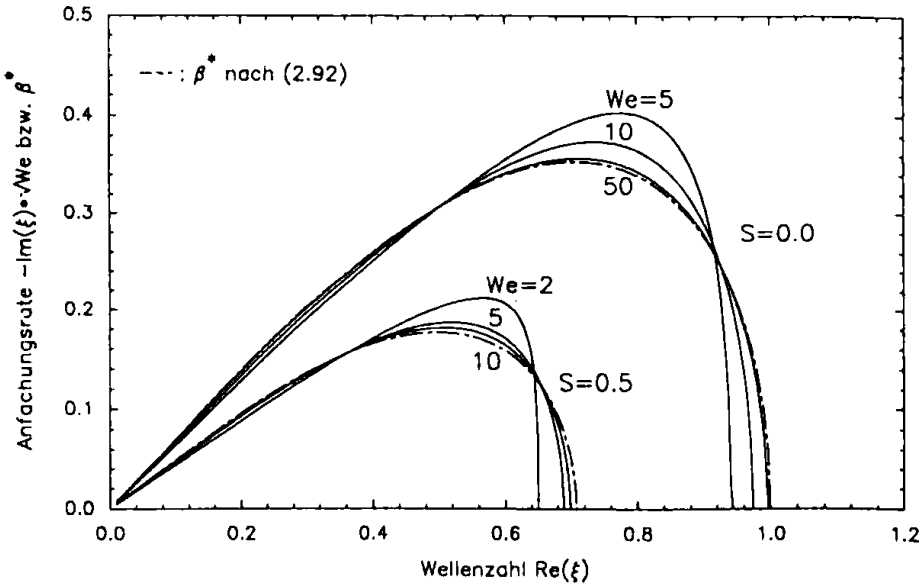

Figure 12: Spatial growth rate for $S = 0$ and 0.5 according to (117). Translator's note: *Anfachungsrate* — $\Im(\xi) \cdot \mathrm{We}^{1/2}$ *bzw.* β^* = *growth rate* — $\Im(\xi) \cdot \mathrm{We}^{1/2}$ *or* β^*, *Wellenzahl* = *wavenumber*, and *nach* = *according to*.

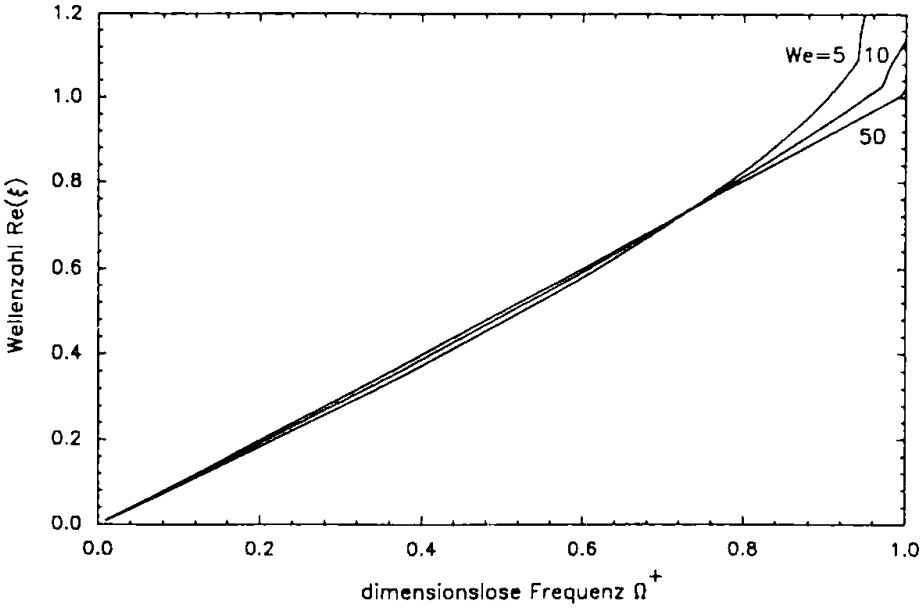

Figure 13: Wavenumber over dimensionless frequency for $S = 0$ according to (116). Translator's note: *Wellenzahl* = *wavenumber* and *dimensionslose Frequenz* = *dimensionless frequency*.

2.3.1 Theoretical wave growth near the nozzle

With regard to the experimental part of the work, the convective wave growth near the nozzle is of particular interest. It is theoretically described by (107), where the general solution is the sum of the four individual solutions to the roots ξ_1 to ξ_4 of (112). However, the two above non-physical solutions with $|\xi| \sim (2\mathrm{We})^{1/2}$ not taken into account. Then, in complex notation p. 49

$$\eta = \mathrm{e}^{-\mathrm{i}\Omega t}\left(C_1\mathrm{e}^{-\mathrm{i}\xi\zeta} + C_2\mathrm{e}^{-\mathrm{i}\overline{\xi}\zeta}\right) \quad \text{with} \quad \zeta = z/R, \tag{120}$$

use was made of the fact that the two remaining roots are complex conjugated in the unstable wavenumber range. Let ξ be the root with the negative imaginary part, which describes the unstable part of the solution, and $\overline{\xi}$ be the root of the decaying part. The kinematic boundary condition at the nozzle outlet

$$\eta(\zeta = 0) = 0 \tag{121}$$

which leads to $C_2 = -C_1$, and you can write with $C_1 = \eta_0$: p. 50

$$\eta = \eta_0\mathrm{e}^{-\mathrm{i}\Omega t}\left[\mathrm{e}^{-\mathrm{i}\xi\zeta} - \mathrm{e}^{-\mathrm{i}\overline{\xi}\zeta}\right] = \eta_0\mathrm{e}^{\mathrm{i}(\xi_\mathrm{R}\zeta-\Omega t)}2\sinh(-\xi_\mathrm{I}\zeta) \quad (\xi_\mathrm{I} < 0!). \tag{122}$$

The still free constant η_0 is determined from the speed disturbances at the nozzle outlet. To do this, write (103) using (108) for the two solution parts and add them up. You get:

$$\frac{u^{(1)}}{U} = 2\frac{\eta_0}{R}\mathrm{e}^{-\mathrm{i}\Omega t}\left\{\Omega^+\left[\mathrm{e}^{\mathrm{i}\xi\zeta}/\xi - \mathrm{e}^{\mathrm{i}\overline{\xi}\zeta}/\overline{\xi}\right] - \left[\mathrm{e}^{\mathrm{i}\xi\zeta} - \mathrm{e}^{\mathrm{i}\overline{\xi}\zeta}\right]\right\}. \tag{123}$$

One sets for the velocity fluctuations at the nozzle outlet

$$u^{(1)}(\zeta = 0, t) = \hat{U}\mathrm{e}^{-\mathrm{i}\Omega t}, \tag{124}$$

follows from this Check

$$\frac{\hat{U}}{U} = 2\frac{\eta_0}{R}\Omega^+(1/\xi - 1/\overline{\xi}) = -4\mathrm{i}\frac{\eta_0}{R}\Omega^+\frac{\xi_\mathrm{I}}{\xi_\mathrm{R}^2 + \xi_\mathrm{I}^2}. \tag{125}$$

This equation describes the relationship between the constant η_0/R and the relative speed disturbances at the nozzle outlet. If you replace η_0 in (122), you get the relationship

$$\frac{\eta}{R} = \frac{\hat{U}}{U}\mathrm{e}^{\mathrm{i}(\xi_\mathrm{R}\zeta-\Omega t)}\frac{\mathrm{i}}{2}\frac{\xi_\mathrm{R}^2 + \xi_\mathrm{I}^2}{\Omega^+\xi_\mathrm{I}}\sinh(-\xi_\mathrm{I}\zeta), \tag{126}$$

in which ξ_R and ξ_I can still be used explicitly for the important special case of very large Weber numbers. For We $\to \infty$ the following applies according to (118) and (119) $\xi_R = \Omega^+$ and $\xi_I = -\beta^*/\mathrm{We}^{1/2}$ so that you can write:

$$\frac{\eta}{R} \approx \frac{\hat{U}}{U}\mathrm{We}^{1/2}\mathrm{e}^{\mathrm{i}\Omega(z/U-t)}\,\frac{\mathrm{i}}{2}\frac{\Omega^+}{\beta^*}\sinh\left[\frac{\beta^*\zeta}{\mathrm{We}^{1/2}}\right]. \tag{127}$$

The surface waves therefore grow near the nozzle according to the hyperbolic sine function. Only for big arguments $\beta^*\zeta/\mathrm{We}^{1/2}$, i.e. generally large nozzle distances, this becomes an exponential curve.

The term p. 51

$$\frac{\hat{U}}{U}\mathrm{We}^{1/2} = \frac{\hat{U}}{\sqrt{\sigma/(\rho R)}} \tag{128}$$

in (127) corresponds to the perturbation of the nozzle exit velocity related to the reference velocity $\sqrt{\sigma/(\rho R)}$ and is common in the literature[25].

2.4 Numerical calculation

In this section the nonlinear problem of wave development described by the continuity equation (94) p. 52
and the momentum equation (100) is solved numerically.[26]

The difference in the turbulent normal stresses contained in (100) is again expressed with the help of the RDT as a function of the jet expansion c:

$$\overline{u_z'^2} - \overline{u_r'^2} = \frac{\overline{u_z'^2}}{\overline{u_z'^2}^{(0)}}U^2T_{zz} - \frac{\overline{u_r'^2}}{\overline{u_r'^2}^{(0)}}U^2T_{rr} = U^2T_{zz}\left[\frac{\mu_z(cc_\mathrm{v})}{\mu_z(c_\mathrm{v})} - \frac{1}{A}\frac{\mu_r(cc_\mathrm{v})}{\mu_r(c_\mathrm{v})}\right], \tag{129}$$

where $\overline{u_z'^2}^{(0)} = U^2T_{zz}$ and $\overline{u_r'^2}^{(0)} = U^2T_{rr} = U^2T_{zz}/A$ are the square mean values of the fluctuation velocities in the undeformed jet and μ_z, μ_r are the functions according to (72) and (73). The axial jet expansion c is calculated from (76); the virtual strain c_v from (79).

Because of the increasing disintegration of turbulence with increasing nozzle spacing, T_{zz} is a function of z, as discussed in sec. 1.4 at the beginning. This function $T_{zz}(z)$ and possibly also $A(z)$ are unknown. It would be possible to use an approach like (69), but it is not known to what extent it applies to the turbulence structure in the jet. Instead, the constancy of the turbulence parameters is

[25] See Bousfield, Stockel, and Nanivadekar [BSN90].

[26] The approach here corresponds to that of Lee [Lee74], who solves the nonlinear, quasi-one-dimensional problem in the case of a inviscid, non-turbulent flow using a Lax-Wendroff method (see e.g. Mitchell [Mit77]).

still assumed. This may not correspond to the actual conditions during the breakup process, but it does provide information about the non-linear influence of turbulence on the formation of waves, whereby the waveform is of particular interest.

The dimension-dependent variables r_s and $u(z,t)$ are replaced by the following dimensionless quantities for the numerical solution:

$$f(\zeta, t^*) = u/\sqrt{\frac{\sigma}{\rho R}}, \tag{130}$$

$$g(\zeta, t^*) = r_s/R, \tag{131}$$

with

$$\zeta = z/R, \tag{132}$$

$$t^* = t/\sqrt{\frac{\rho R^3}{\sigma}}. \tag{133}$$

I.e. the reference length is R, and the reference time and speed are Check

$$\tau_{\text{ref}} = \sqrt{\frac{\rho R^3}{\sigma}}, \tag{134}$$

$$U_{\text{ref}} = R/\tau_{\text{ref}} = \sqrt{\frac{\rho}{\sigma R}}. \tag{135}$$

Inserting of (129) to (133) in (94) and (100), the differential equation system returns[27]

$$\dot{g} + f\, g' + \frac{1}{2} g\, f' = 0, \tag{136}$$

$$\dot{f} + f\, f' = -\frac{\partial \kappa}{\partial \zeta} - S_0\, F_{\text{T}}, \tag{137}$$

where κ is the related surface curvature according to (33), which is written in g as

$$\kappa = R\left[\frac{1}{R_1} + \frac{1}{R_2}\right] = \frac{1}{(1+g'^2)^{1/2}}\left[\frac{1}{g} - \frac{g''}{1+g'^2}\right]. \tag{138}$$

[27]Here and further, $(\dot{})$ and $(\,)'$ stand for the partial derivatives according to the dimensionless coordinates t^* and ζ.

The turbulence term $S_0\, F_\mathrm{T}$ in (137) is composed of the function

$$F_\mathrm{T} = \frac{5}{6}\left[\left[\frac{\mu_z(cc_\mathrm{v})}{\mu_z(c_\mathrm{v})} - \frac{1}{A}\frac{\mu_r(cc_\mathrm{v})}{\mu_r(c_\mathrm{v})}\right]\left[\frac{1}{g} + \frac{g''}{1+g'^2}\right] - c_\mathrm{v}\left[\frac{\mu_z(cc_\mathrm{v})}{\mu_z'(c_\mathrm{v})} - \frac{1}{A}\frac{\mu_r'(cc_\mathrm{v})}{\mu_r(c_\mathrm{v})}\right]\frac{1}{g^3}\right] \tag{139}$$

and the turbulence parameter S_0 according to (90). The turbulence function F_T has the property, for small deformations and the special case of isotropic turbulence, on the simple formula

$$F_\mathrm{T} \to g' \quad \text{for} \quad g \to 1 \quad \text{and} \quad g' \to 0 \tag{140}$$

respectively. The argument of μ_z, μ_r, μ_z' and μ_r' is because of (76), (80)

$$c_\mathrm{ges} = c_\mathrm{v} c = c_\mathrm{v}/g^2. \tag{141}$$

The solution interval of (136) and (137) initially extends over the complete jet length, which is a multiple of the wavelength of the surface disturbances.

Apart from the problems that arise in connection with a previously unknown jet length, the solution of the differential equations at this interval would mean an enormous numerical effort, since the spatial discretization must be chosen so fine that the surface waves also in the stage shortly before breakup can still be resolved sufficiently. Therefore, the simpler model of spatially periodic disturbances is to be assumed here, the results of which, as shown in Sec. 2.3, can be directly converted into a spatial development with temporal periodicity for large Weber numbers. A coordinate system is then expediently chosen which moves at the base flow rate U, so that the undisturbed solution is $g = 1$, $f = 0$. This enables the solution interval to be reduced to a wavelength λ of the initial disturbance to be specified. The boundary conditions for the solution of (136) and (137) are then periodicity conditions. If the perturbations for $t^* = 0$ are symmetrical or antisymmetric to the middle of the interval $z = \lambda/2$, they remain in the absence of any asymmetrical influences for $t^* > 0$, and the solution interval can continue be limited to half a wavelength. p. 54 Check

In order to be able to use this advantage, the function $g(\zeta, t^*)$ as symmetrical and $f(\zeta, t^*)$ as antisymmetric is furthermore changed to $\zeta = 0$ and $\zeta = \lambda/(2R)$ provided that this is sketched in

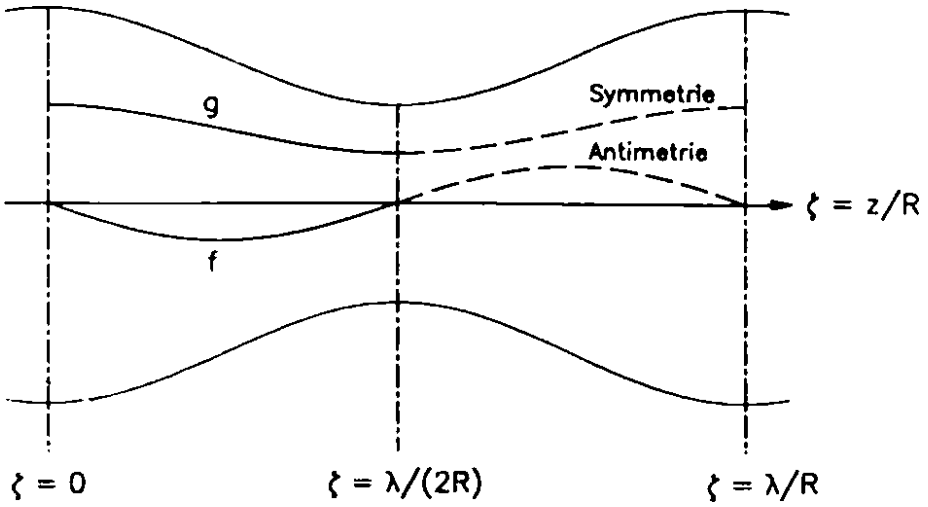

Figure 14: Solution interval and initial conditions. Translator's note: *Symmetrie* = *symmetry* and *Antimetrie* = *antisymmetry*.

figure 14. The periodicity conditions are then

$$g(-\zeta) = g(\zeta) \quad \text{and} \quad g(\lambda/(2R) - \zeta) = g(\lambda/(2R) + \zeta), \tag{142}$$

$$f(-\zeta) = -f(\zeta) \quad \text{and} \quad f(\lambda/(2R) - \zeta) = -f(\lambda/(2R) + \zeta). \tag{143}$$

Compatible initial conditions are because of $\xi = 2\pi R/\lambda$ p. 55

$$g(\zeta, t^* = 0) = 1 + \hat{g}_0 \cos(\xi\zeta), \tag{144}$$

$$f(\zeta, t^* = 0) = -\hat{f}_0 \sin(\xi\zeta). \tag{145}$$

The amplitudes $\hat{g}_0$ and $\hat{f}_0$ are freely selectable. You can e.g. recover from the solution of the linear problem, for which the differential equations (136) to (139) are simplified: Check

$$\dot{g} + \frac{1}{2} f' = 0, \tag{146}$$

$$\dot{f} = g' + g''' - S_0 g' \quad (\text{for } A = 1). \tag{147}$$

2.4.1 Numerical method

The algorithm for the numerical solution works as follows: First, the required spatial derivatives (f', g', g'' and g''') with the usual difference quotients[28]

$$\begin{bmatrix} g'_k & \Delta\zeta \\ g''_k & \Delta\zeta^2 \\ g'''_k & \Delta\zeta^3 \end{bmatrix} = \begin{bmatrix} 1/12 & -8/12 & 0 & 8/12 & -1/12 \\ -1/12 & 16/12 & -30/12 & 16/12 & -1/12 \\ -1/2 & 2/2 & 0 & -2/2 & 1/2 \end{bmatrix} \begin{bmatrix} g_{k-2} \\ g_{k-1} \\ g_k \\ g_{k+1} \\ g_{k+2} \end{bmatrix} + O(\Delta\zeta^2) \tag{148}$$

(correspondingly also for f) with equidistant grid points ζ_k, $k = 1$ to N, approximated between $\zeta = 0$ and $\zeta = \pi/\xi$. The resulting system of $2N$ coupled, ordinary differential equations in t^* is then integrated using an implicit 3rd order Runge-Kutta method of the Gauss type.[29]

While the initial conditions (144), (145) and the linear solutions discussed in the previous sections are purely harmonic, the solution of the nonlinear problem naturally loses this property. In addition to the fundamental vibrations with the wavelength λ there are harmonics with $\lambda/2$, $\lambda/3$ etc. The decomposition of the jet deformation into such Fourier components is the basis of most analytical stability theories of higher order[30]. In order to obtain information about the existence of higher harmonic waves, the solution $g(\zeta, t) - 1 = (r_s - R)/R$ numerically calculated at equidistant points in ζ and t^* is then subjected to a Fourier transformation: p. 56

$$G_\nu(t^*) = \frac{\xi}{2\pi} \int_0^{2\pi/\xi} \mathrm{e}^{-\mathrm{i}\nu\xi\zeta} \{g(\zeta, t^*) - 1\} \, \mathrm{d}\zeta. \tag{149}$$

Since g is an even function, the result is purely real, and the inverse of (149) is

$$g(\zeta, t^*) = 1 + \sum_{\nu=-\infty}^{\infty} G_\nu(t^*) \cos(\nu\xi\zeta) = 1 + G_0(t^*) + 2 \sum_{\nu=1}^{\infty} G_\nu(t^*) \cos(\nu\xi\zeta). \tag{150}$$

The integrals in (149) are calculated for $\nu = 0, 1, 2,$ to 10 using Simpson's rule. The solution is completed by mirroring the entire interval $\zeta = 0$ to $2\pi/\xi$. Check

Since there is no mass flow over the areas $\zeta = 0$ and $\zeta = 2\pi/\xi$, for reasons of continuity, this

[28] See e.g. Engeln-Müllges, Reutter, and Axmacher [ERA76, pp. 387–395].

[29] The procedure largely corresponds to the "Method of Lines", see Loeb and Schiesser [LS74].

[30] See, e.g. Yuen [Yue68] and Chaudhary and Redekopp [CR80].

must be done by the integral

$$\frac{V}{\pi R^2 \lambda} = \frac{1}{2\pi/\xi} \int_0^{2\pi/\xi} g^2(\zeta, t^*)\, \mathrm{d}\zeta \tag{151}$$

given dimensionless volumes that are the same for each time step. With corresponding initial disturbances, this constant value is one. This condition is used as a necessary control condition for the numerical method. (The deviations that occurred in the calculations carried out always remained below 0.05%.)

The number of sampling points in ζ was chosen with $N = 51$. The higher this number, the closer to the breakup point can be calculated. For the initial stage of the process, where $g = r_S/R$ does not deviate significantly from the value one, a much coarser spatial discretization is sufficient. The "breakup point" is reached numerically if it is not possible to integrate from one time step t_i^* to the next t_{i+1}^*. p. 57

2.4.2 Results for laminar jets

Figure 15 to 19 initially show the results for a laminar jet ($S_0 = S = 0$) with a wave number of $\xi = 0.7$, which corresponds to the maximum fanned wave number according to figure 9. In the initial condition (144), (145) was set to Check

$$\hat{g}_0 = \epsilon_0 = 2 \cdot 10^{-2}, \quad \hat{f}_0 = \epsilon_0 \sqrt{2(1 - \xi^2 - S)}. \tag{152}$$

The ratio of the initial interference amplitudes in g and f corresponds to the result of the linear theory according to (103) if one converts the latter to the coordinate system used here, which moves with the base flow.

As the development of the jet radius in figure 15 and especially the speed in figure 16 show, for $t^* \approx 10.25$ there is a very sudden pinching off of the jet. Although the underlying one-dimensional theory cannot of course exactly reproduce the strong spatial flow immediately before breakup, it is nevertheless able to reproduce the well-known phenomenon of so-called satellite drop formation. The jet is not constricted at $z = \lambda/2$, i.e. in the middle between two wave crests, but a local maximum is formed there. The first separation of the jet lies between a wave crest and this local maximum, in the example here around $z/(\lambda/2) = 0.52$. The result of this, which is easy to observe experimentally, is that even with an initially harmonic disturbance of the jet (at least) two classes of drops arise. The drops from the area of the absolute maximum in figure 15 are usually much larger than the satellite drops that result from the local maximum at $z = \lambda/2$. The more long-wave the disturbances are,

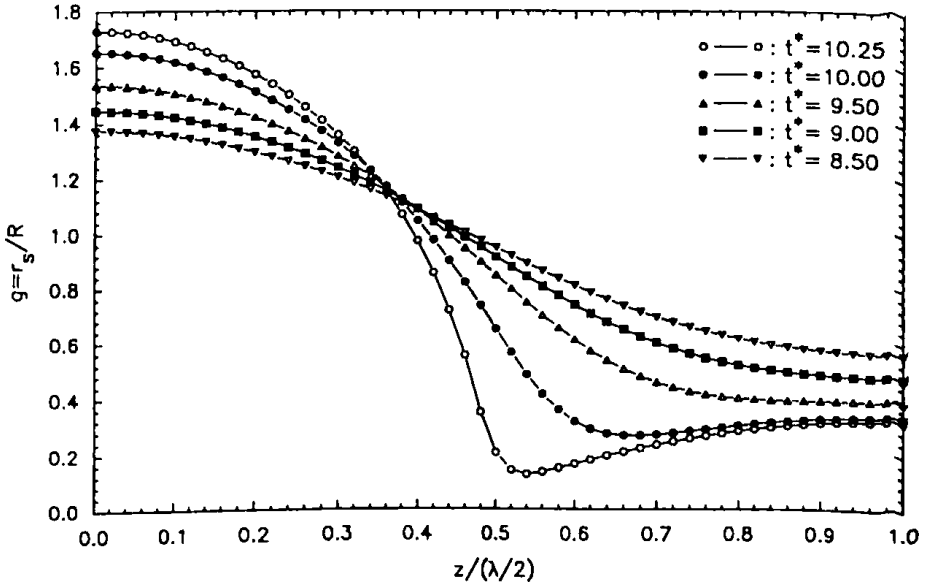

Figure 15: Development of the dimensionless jet radius for $\xi = 0.7, S_0 = 0$.

the more pronounced this phenomenon becomes. In the case of very short-wave ($\xi \to 1$) it finally disappears[31].

Figure 17 shows the temporal development of the wave crests and valleys. For this purpose, the p. 59
largest and smallest values of the dimensionless jet radius g were determined for each time step of the numerical calculation (the deviations from $g = 1$ are shown as circles in figure 17) and then the difference $g_{\max} - g_{\min}$ formed (triangles). Also shown is the corresponding course of the linear theory, which forms a straight line on a semi-logarithmic scale. While the points of the minima and maxima do not lie on a straight line, the calculation points of the differences do so with surprising accuracy. That the distance between wave crests and valleys practically follows the exponential law of linear theory up to the breakup point![32] A different picture emerges from other wave numbers than that of the example under consideration, but the non-linear courses sometimes differ somewhat earlier from the linear ones.

Figure 18 shows the numerically calculated curves of the Fourier components according to (149) on a linear scale; Figure 19 shows their amounts on a semi-logarithmic scale. Although the coefficients $G_\nu(t_i^*)$ were calculated for $\nu = 0$ to 10, only the first four ($\nu = 0$ to 3) are shown, but it

[31]This result is consistent with the analytical work by Yuen [Yue68] (3rd order nonlinear perturbation calculation) and the numerical work by Lee [Lee74].

[32]As Yuen's theory [Yue68] shows, in the difference of the extrema the nonlinear terms up to and including the quadratic order are dropped.

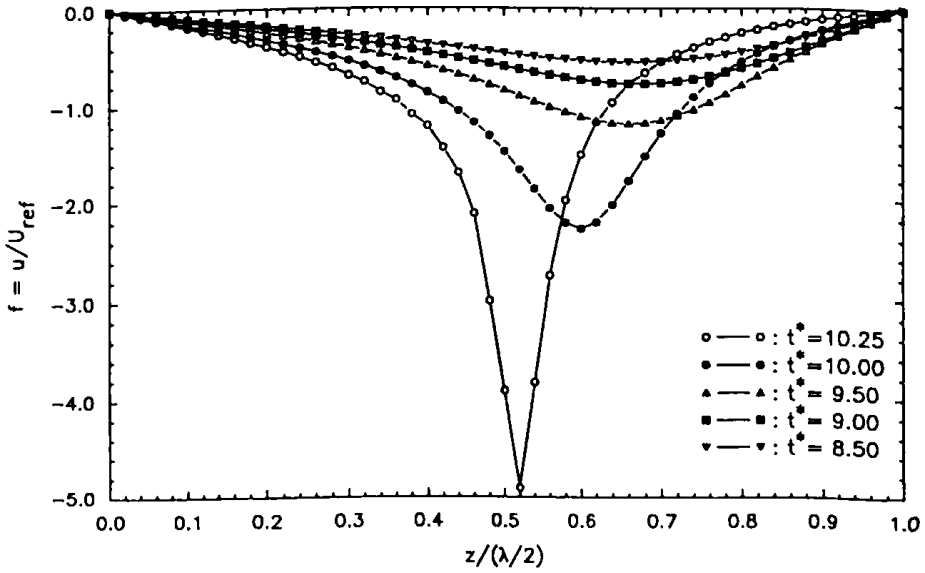

Figure 16: Development of the dimensionless jet velocity for $\xi = 0.7, S_0 = 0$.

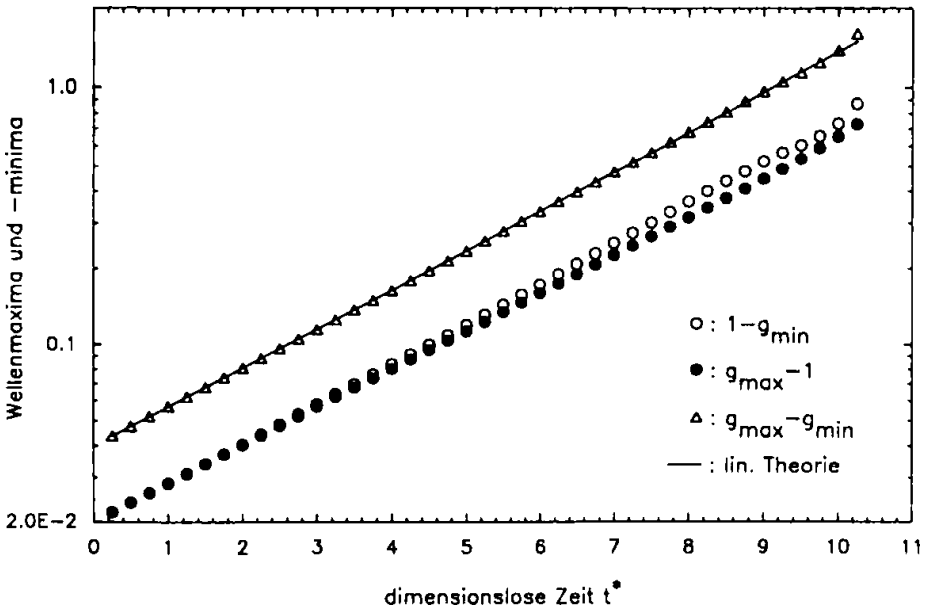

Figure 17: Time course of the wave crests and valleys for $\xi = 0.7, S_0 = 0$ and comparison with the linear theory. Translator's note: *Wellenmaxima und —minima = wave crests and valleys* and *dimensionslose Zeit = dimensionless time*.

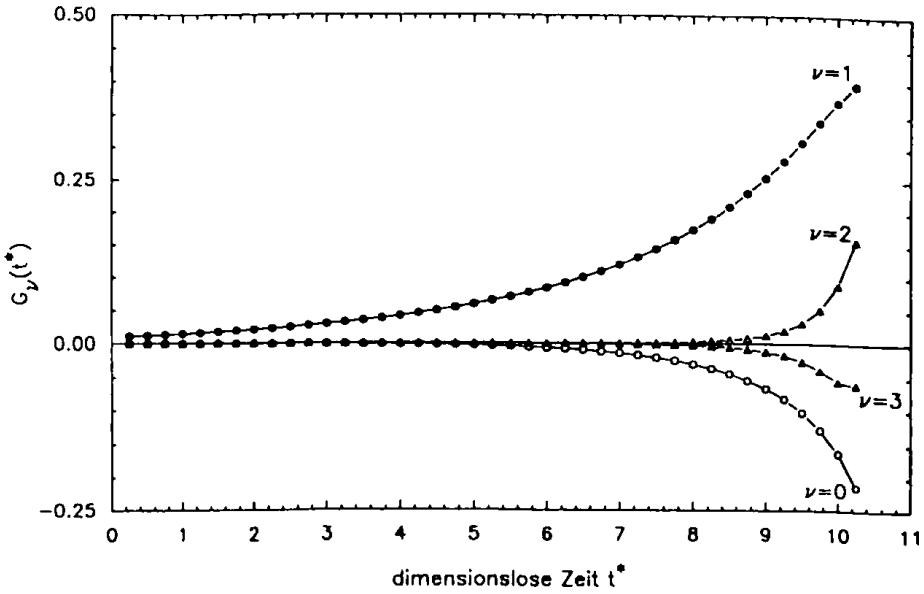

Figure 18: Time course of the first four Fourier components of the radius change for $\xi = 0.7, S_0 = 0$ in a linear representation. Translator's note: *dimensionslose Zeit = dimensionless time*.

should be noted that immediately before breakup, the higher proportions also assume significant sizes.

In the early stage of breakup, the component of the constant component G_0 dominates in addition p. 61
to the fundamental vibration G_1. This is because the increase in volume due to a positive shift in the jet radius is greater than the decrease in volume due to a negative shift in the same amount. For reasons of continuity, therefore, a cosine wave of finite amplitude (G_1) is accompanied by a negative constant shift (G_0).

Only when G_1 exceeds the value 0.25 (the full amplitude of the fundamental is then according to (150) $2 \cdot G_1 = 0.5$), do the first two harmonics reach G_2 and G_3 worth mentioning orders of magnitude. In the case of long-wave interference, this is the case a little earlier.

Before going into the results for turbulent rays, first consider the initial condition (152). As mentioned, this initial condition was chosen so that it conforms to the linear solution according to (103). In sec. 2.3, however, convectively unstable waves were considered, in which the disturbances of g at the nozzle outlet ($z = 0$) disappear and the initial disturbances are pure speed vibrations. These waves can also be calculated numerically using the described method. The transformation $z = Ut$ (see figure 11) is used for this and for $t = 0$ (i.e. $z = 0$) the initial condition $g = 1$, i.e. $g = 0$, and $f = -\hat{f}_0 \sin(\xi\zeta)$ prescribed. As shown in sec. 2.3, this conversion is allowed for large Weber

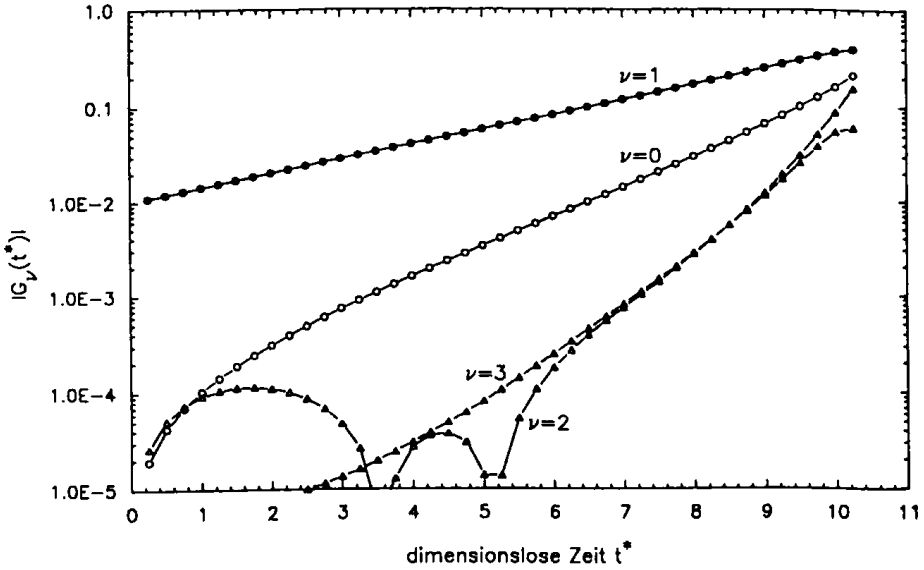

Figure 19: Time course of the amounts of the first four Fourier components of the radius change for $\xi = 0.7, S_0 = 0$ in a semi-logarithmic representation. Translator's note: *dimensionslose Zeit* = *dimensionless time*.

numbers (We $>$ 10 to 50).

Because of the simpler comparison with the solution resulting from the initial condition (152), the amplitude $\hat{f}_0$ should first be determined so that for $t^* \gg 1$ both solutions merge into the same curve. According to (113), (116), (125) and (128) this is the case for large Weber numbers when the amplitude of the speed disturbance is twice as large as in (152). The initial conditions are then

$$\hat{g}_0 = 0, \quad \hat{f}_0 = 2\epsilon_0\sqrt{2(1-\xi^2-S)} \quad (\epsilon_0 = 2 \cdot 10^{-2}). \tag{153}$$

Figure 20 shows the course of the distance between the wave extrema $g_{\max} - g_{\min}$ on a semi-logarithmic scale. The triangles of the lower curve represent the values of the numerical calculation for the initial condition(153), while the course of the initial condition (152) is drawn in again for comparison purposes. The corresponding curves of linear theory are also shown, namely on the one hand the straight line of the purely exponential law and on the other hand the curve resulting from the solution (127). Two things can be seen: Firstly, the good agreement between numerical results and linear theory in the area of small disturbances proves that the transformation of the spatial coordinate p. 62
z to the time coordinate t on which the numerical calculation is based is a very good approximation. Secondly, it becomes clear that the choice of the initial conditions obviously only has an effect in a

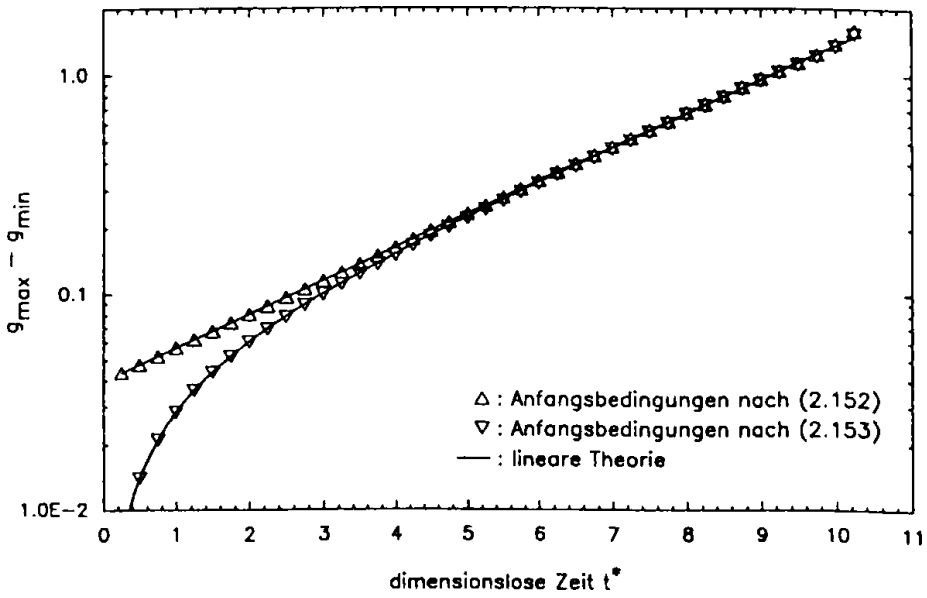

Figure 20: Wave development under different initial conditions and comparison with linear theory ($\xi = 0.7, S_0 = 0$). Translator's note: *Anfangsbedingungen nach* = *initial conditions after*, *lineare Theorie* = *linear theory*, and *dimensionslose Zeit* = *dimensionless time*.

transition area. If the initial disturbance level is not too high, the dynamics of the jet breakup beyond this transition area are completely independent of the conditions at the nozzle outlet.[33]

2.4.3 Turbulent jets

While the solution discussed above for the laminar case depends only on the wave number ξ, for $S_0 \neq 0$ the dimensionless parameters ξ, S_0 and $A = T_{zz}/T_{rr}$. First, however, considerations are limited to *isotropic turbulence* in the undeformed jet ($A = 1$). Then S_0 is identical to the parameter S used in linear theory (see figure 8) and is therefore not distinguished from this in the following.

In order to study the influence of turbulence on the non-linear wave development, the calculation described above is repeated several times. All parameters remain constant, only the turbulence parameter is gradually increased from 0 until wave growth no longer occurs.

The growth rates of the linear theory shown in figure 9 serve as a guide for the range of values of S in question. For a wave number of $\xi = 0.7$, turbulence parameters in the range $0 \leq S \leq 1 - 0.7^2 = 0.51$ should lead to unstable waves. Check p. 64

[33] See Torpey [Tor89, p. 666 ff.].

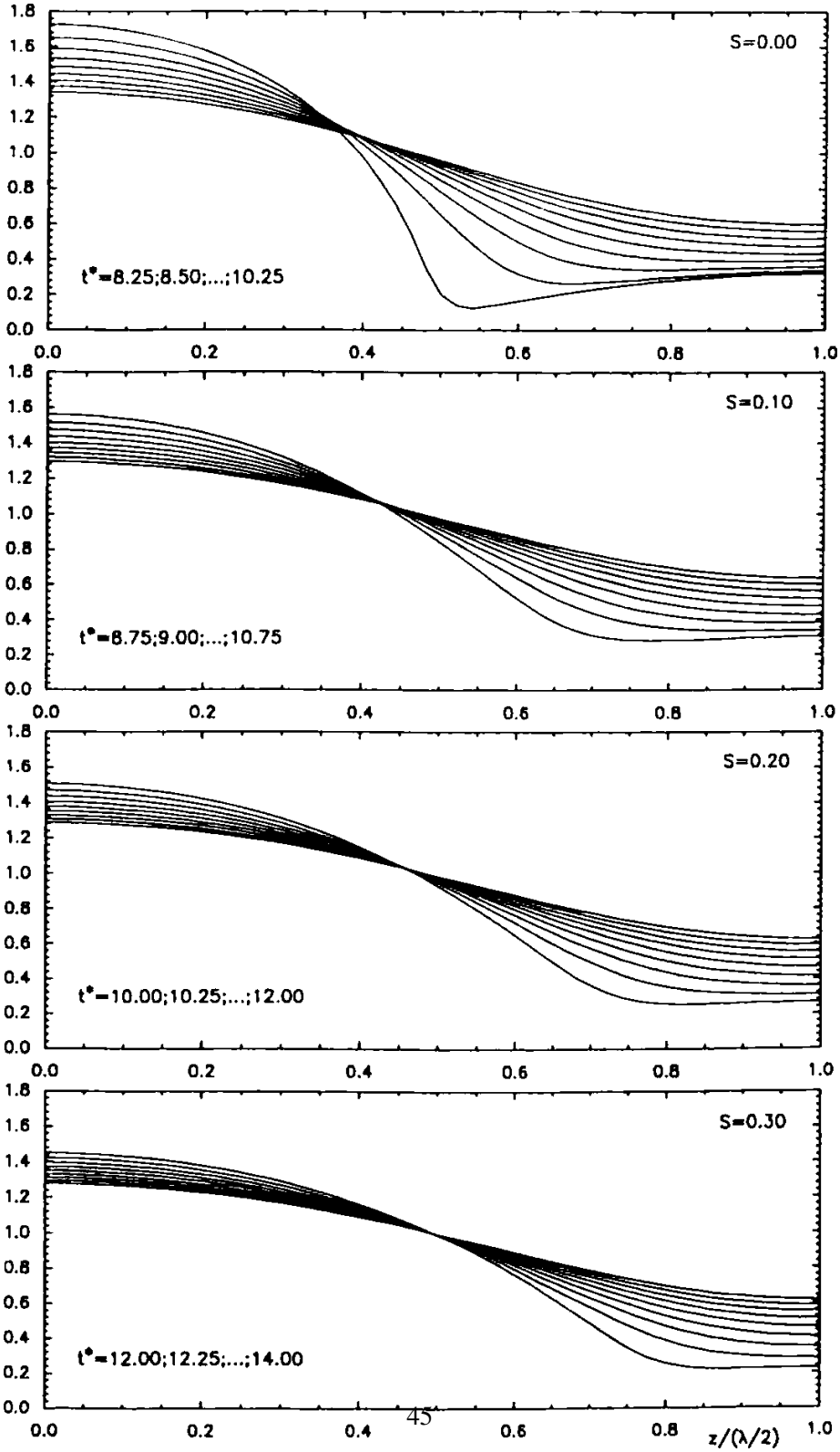

Figure 21: Development of the dimensionless jet radius g for $\xi = 0.7$ and $A = 1$.

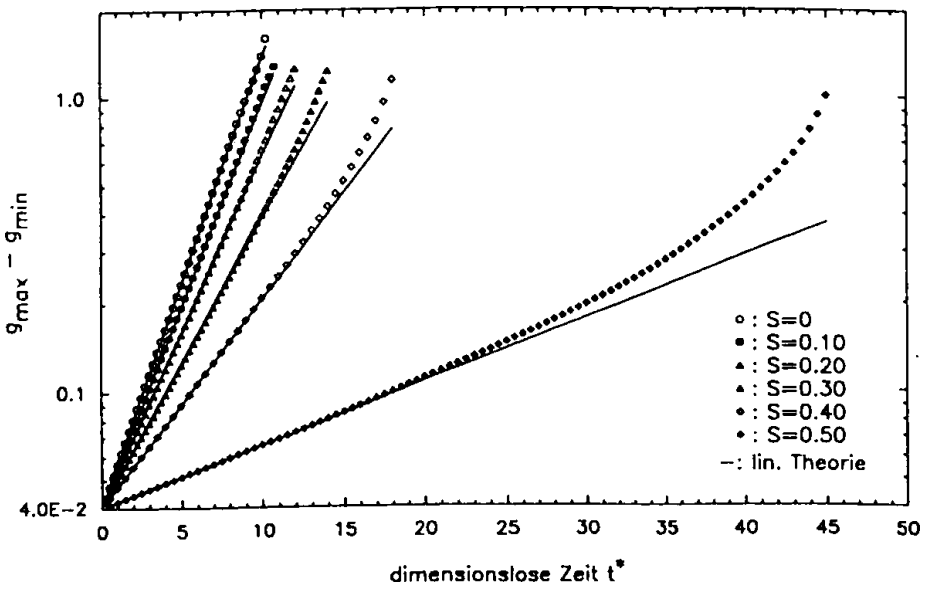

Figure 22: Wave development with different turbulence parameters S ($\xi = 0.7$, $A = 1$). Translator's note: *dimensionslose Zeit = dimensionless time*.

Figure 21 shows for $S = 0$ to 0.3 the effect of the turbulence parameter on the shape of the surface waves. For this, the calculated surface contours are plotted at 9 equidistant times ($\Delta t^* = 0.25$), whereby the last time always corresponds to that of the last successful time step.

A very clear effect of turbulence is the reduction in the size of the satellite drops by shifting the jet radius minimum in the direction of $z = \lambda/2$. As a result, the height of the wave crest decreases and the jet deformation appears longer cosine. The increase in the breakup time with increasing S under the same initial conditions according to (152) confirms the statement of the linear theory: Turbulence has a stabilizing effect on rotationally symmetrical waves. The laminar jet decays after a time of $t^* = 10.25$ and the turbulent jet with $S = 0.3$ only at $t^* = 14.00$. The results for $S = 0.4$ and 0.5, not shown in figure 21, yield breakup times of $t^* = 18$ and 45, respectively. As expected, there was no wave growth for $S > 0.5$ because the numerical calculation was started from the linear range.

Figure 22 shows, as for the laminar case (figures 17 and 20), the temporal development of the p. 65
difference in height between wave crests and valleys. For comparison, the linear properties according to (92) are also shown again. In line with linear stability theory, the larger S is, the flatter the slope of the curves. Because of the steep drop in the growth rates in the vicinity of the stability limit according to figure 9, this effect becomes particularly great if one approaches the limit of 0.51 valid for $\xi = 0.7$.

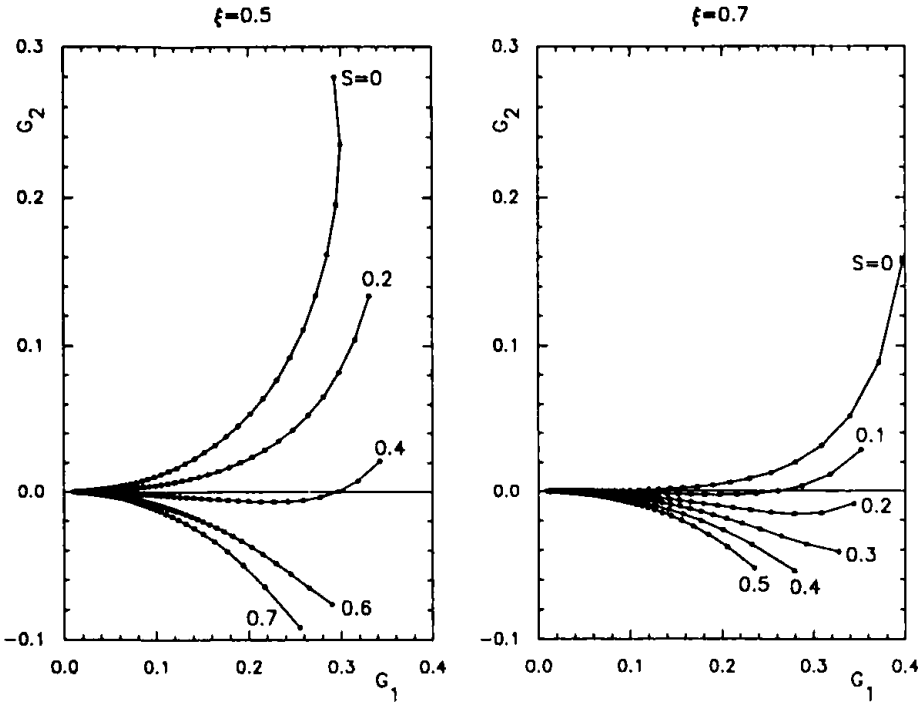

Figure 23: Relationship between the Fourier components of the fundamental and first harmonic depending on the turbulence parameter S ($A = 1$).

It should also be noted that the deviations between the non-linear solutions and the straight lines of the linear stability theory increase with increasing S. While linear and non-linear solutions are practically coincident up to the breakup point for $S \to 0$, the waves grow significantly faster at higher turbulence values in the late stage of breakup than the linear theory predicts. The curves of figure 22 even give the impression that the slope immediately before breakup is almost independent of the turbulence parameter S, i.e. always approximately as large as in the laminar case. Obviously, the process of pinching off drops is characterized solely by the action of capillary tension.

In figure 23 for the wave numbers $\xi = 0.5$ and $\xi = 0.7$ the Fourier component of the first harmonic G_2 is plotted against that of the fundamental vibration G_1. The curve parameter, not shown, is therefore the time t^*. The result confirms the statement made in connection with figure 21: The turbulence reduces G_2. While large positive harmonic amplitudes occur especially for $S = 0$ shortly before breakup, they disappear at medium turbulence values and finally become negative at large ones, but then do not reach the same amount. With small wave numbers, the higher Fourier components due to nonlinearities are larger overall than with large ones, which can be explained by p. 66

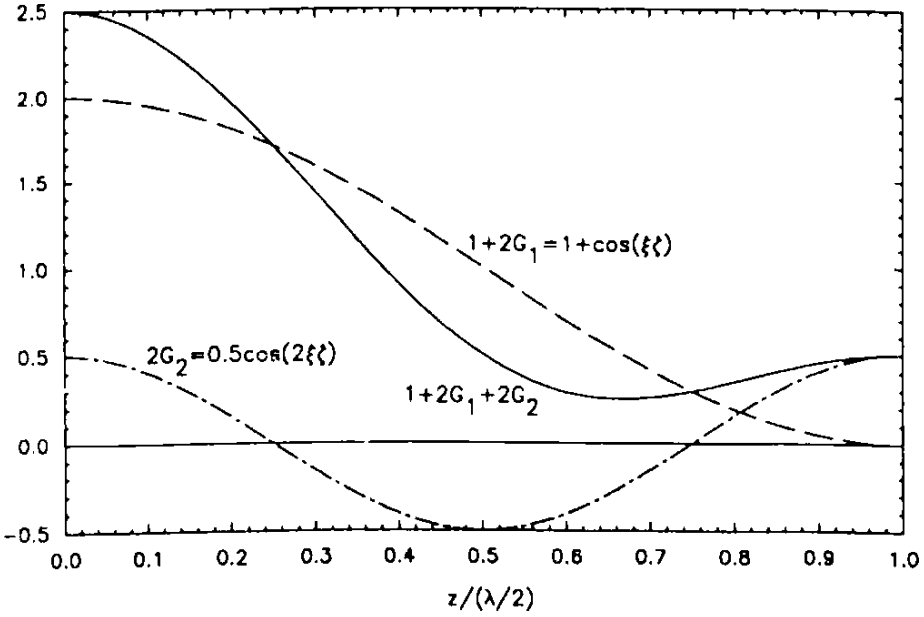

Figure 24: Qualitative generation of the typical appearance of the contour of a laminar jet by superimposing a fundamental wave with a harmonic of double wave number and half amplitude.

the known phenomenon of web formation between the wave crests.

Figure 24 illustrates the effect of reducing G_2: The characteristic appearance of the contour of the laminar jet shown in figure 15, for example, can be qualitatively generated by superimposing a cosine wave with a harmonic of double the wave number and half the amplitude. As can be seen, a positive Fourier component G_2 is responsible for pinching off the satellite drops, whereas negative G_2 values make this surprising.

The completely different appearance of laminar and turbulent cases of breakup is illustrated by the comparison in figure 25[34]. The numerically calculated contours of laminar jets ($S = 0$) with the four wave numbers $\xi = 0.25, 0.5, 0.7$ and 0.85 are shown on the left. The times t^* are those of the last time step before the "numerical pinching off"; served as the initial condition (152). To the right are the contours of the turbulent jets with, apart from S, identical parameter values. The laminar jet contours have the typical ridges between two round drops that are formed, especially at long wavelengths ($\lambda/R = 2\pi/\xi$). In the turbulent case, the length of these webs is considerably reduced, and even almost zero for large wavenumbers.

p. 67

Check

Check

[34]The contours calculated for the laminar case are in good agreement with the photographs by Goedde and Yuen [GY70]. Compare in particular the case $\xi = 0.25, S = 0$ of figure 25 with the illustration on p. 503 of the cited work. For the comparison with own measurements, see section 4.1.3.

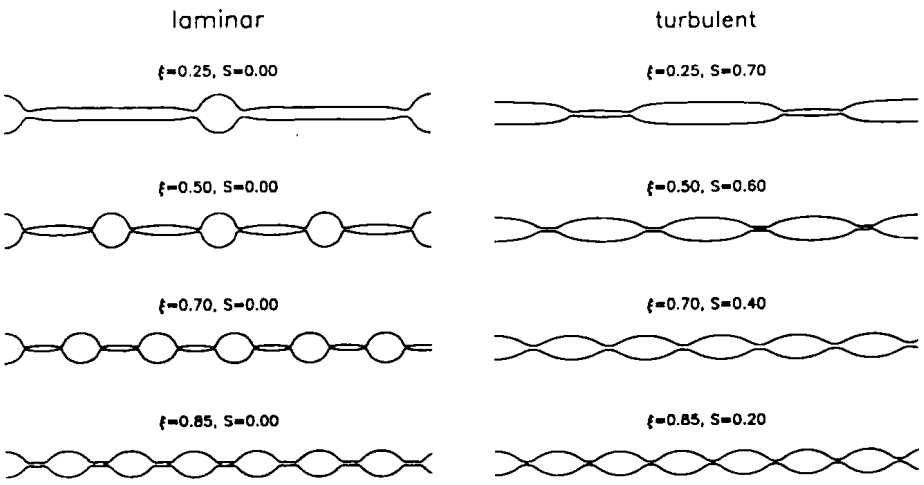

Figure 25: Comparison of the numerically calculated jet contours shortly before breakup in scale representation ($A = 1$).

2.4.4 Influence of anisotropy

The last point to be examined is the influence of anisotropy. While in the linear theory a change in the anisotropy parameter A was noticeable through a change in S according to figure 8, A is included in the numerical calculation of the virtual strain c_v in the turbulence function (139) into the solution. p. 68

The decrease in S with increasing A resulted in a decrease in the stabilizing influence of turbulence in linear theory. This is also confirmed by the numerical solution of the nonlinear problem. Figure 26 shows for example $\xi = 0.5$ and $S_0 = 0.4$ the influence of A on the wave growth, i.e. the time function $g_{max} - g_{min}$. If the conditions are otherwise the same, the results are can be compared:

$$A = 0.6 \Rightarrow c_v \approx 1.43, S \approx 0.48,$$
$$A = 1.0 \Rightarrow c_v = 1, S = S_0 = 0.4,$$
$$A = 1.6 \Rightarrow c_v \approx 0.57, S \approx 0.31.$$

The effect of anisotropy on the numerical solution of the nonlinear problem is slightly smaller than that of the linear solution. For $A = 1$, $g_{max} - g_{min}$ follows the exponential law of linear theory almost to the breakup point in very good approximation.

The anisotropy levels realized in a turbulent jet are unlikely to exceed the range $0.6 \leq A \leq 1.6$, which is covered in figure 26. As can be seen, the effect of this parameter on the jet stability remains comparatively small, so it is obviously a secondary effect of minor importance.

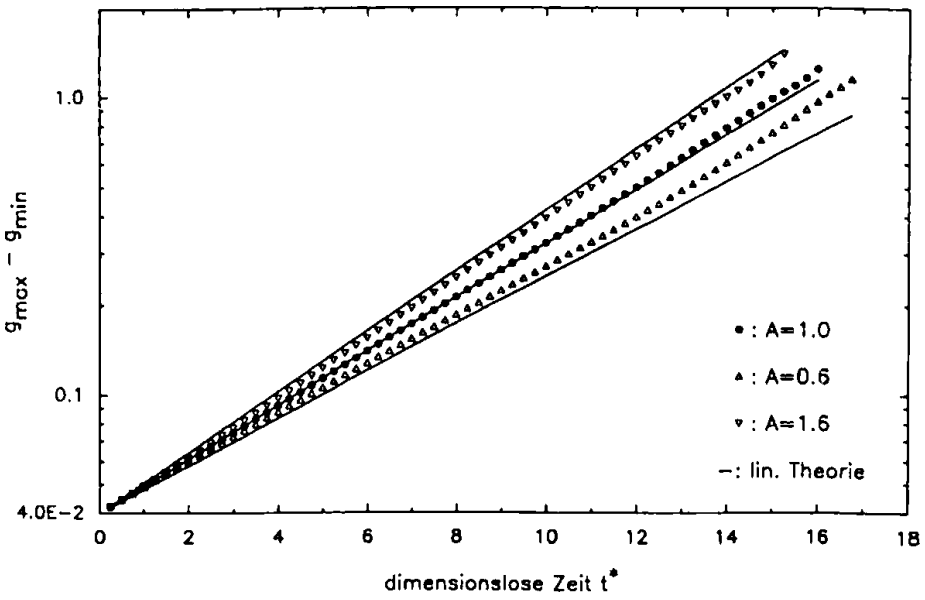

Figure 26: Influence of the anisotropy parameter A on the wave growth ($\xi = 0.5$, $S_0 = 0.4$).

References

[Bat53] G. K. Batchelor. *The Theory of Homogeneous Turbulence*. Cambridge, UK: University Press, 1953. 197 pp. (cit. on pp. 15, 16).

[BP54] G. K. Batchelor and I. Proudman. "The Effect of Rapid Distortion of a Fluid in Turbulent Motion". *The Quarterly Journal of Mechanics and Applied Mathematics* 7(1) (Jan. 1, 1954), pp. 83–103. ISSN: 0033-5614. DOI: 10.1093/qjmam/7.1.83 (cit. on pp. 1, 15).

[BP71] J. S. Bendat and A. G. Piersol. *Random Data: Analysis and Measurement Procedures*. New York, NY: Wiley-Interscience, 1971. 407 pp. ISBN: 978-0-471-06470-1 (cit. on p. 3).

[BSN90] D. W. Bousfield, I. H. Stockel, and C. K. Nanivadekar. "The Breakup of Viscous Jets with Large Velocity Modulations". *Journal of Fluid Mechanics* 218 (Sept. 1990), pp. 601–617. ISSN: 0022-1120. DOI: 10.1017/S0022112090001136 (cit. on p. 34).

[CR80] K. C. Chaudhary and L. G. Redekopp. "The Nonlinear Capillary Instability of a Liquid Jet. Part 1. Theory". *Journal of Fluid Mechanics* 96(2) (Jan. 1980), pp. 257–274. ISSN: 0022-1120. DOI: 10.1017/S0022112080002108 (cit. on p. 38).

[DR04] P. G. Drazin and W. H. Reid. *Hydrodynamic Stability*. 2nd ed. Cambridge University Press, Sept. 20, 2004. 628 pp. ISBN: 978-0-521-52541-1 (cit. on p. 5).

[ERA76] G. Engeln-Müllges, F. Reutter, and D. Axmacher. *Formelsammlung zur numerischen Mathematik*. Mannheim: Bibliographisches Institut, 1976. 373 pp. ISBN: 978-3-411-05106-9 (cit. on p. 38).

[Gas62] M. Gaster. "A Note on the Relation between Temporally-Increasing and Spatially-Increasing Disturbances in Hydrodynamic Stability". *Journal of Fluid Mechanics* 14(2) (Oct. 1962), pp. 222–224. ISSN: 0022-1120. DOI: 10.1017/S0022112062001184 (cit. on p. 29).

[GY70] E. F. Goedde and M. C. Yuen. "Experiments on Liquid Jet Instability". *Journal of Fluid Mechanics* 40(3) (Feb. 1970), pp. 495–511. ISSN: 0022-1120. DOI: 10.1017/S0022112070000289 (cit. on p. 48).

[KRT73] J. B. Keller, S. I. Rubinow, and Y. O. Tu. "Spatial Instability of a Jet". *Physics of Fluids* 16(12) (Dec. 1, 1973), pp. 2052–2055. ISSN: 0031-9171. DOI: 10.1063/1.1694264 (cit. on p. 29).

[Lee74] H. C. Lee. "Drop Formation in a Liquid Jet". *IBM Journal of Research and Development* 18(4) (July 1974), pp. 364–369. ISSN: 0018-8646. DOI: 10.1147/rd.184.0364 (cit. on pp. 34, 40).

[Lew90] J. Lewalle. "Decay of Velocity and Temperature Fluctuations in Grid Turbulence". *AIAA Journal* 28(1) (1990), pp. 106–112. ISSN: 0001-1452. DOI: 10.2514/3.10359 (cit. on p. 16).

[LG86a] S. J. Leib and M. E. Goldstein. "Convective and Absolute Instability of a Viscous Liquid Jet". *Physics of Fluids* 29(4) (Apr. 1, 1986), pp. 952–954. ISSN: 0031-9171. DOI: 10.1063/1.866000 (cit. on p. 29).

[LG86b] S. J. Leib and M. E. Goldstein. "The Generation of Capillary Instabilities on a Liquid Jet". *Journal of Fluid Mechanics* 168 (July 1986), pp. 479–500. ISSN: 0022-1120. DOI: 10.1017/S0022112086000472 (cit. on p. 29).

[LL89] S. P. Lin and Z. W. Lian. "Absolute Instability of a Liquid Jet in a Gas". *Physics of Fluids A: Fluid Dynamics* 1(3) (Mar. 1, 1989), pp. 490–493. ISSN: 0899-8213. DOI: 10.1063/1.857419 (cit. on p. 29).

[LL90] S. P. Lin and Z. W. Lian. “Mechanisms of the Breakup of Liquid Jets”. *AIAA Journal* 28(1) (1990), pp. 120–126. ISSN: 0001-1452. DOI: 10.2514/3.10361 (cit. on p. 29).

[LLC90] S. P. Lin, Z. W. Lian, and B. J. Creighton. “Absolute and Convective Instability of a Liquid Sheet”. *Journal of Fluid Mechanics* 220 (Nov. 1990), pp. 673–689. ISSN: 0022-1120. DOI: 10.1017/S0022112090003421 (cit. on p. 29).

[LS74] A. M. Loeb and W. E. Schiesser. “Stiffness and Accuracy in the Method of Lines Integration of Partial Differential Equations”. *Stiff Differential Systems*. Ed. by R. A. Willoughby. The IBM Research Symposia Series. Boston, MA: Springer US, 1974, pp. 229–243. ISBN: 978-1-4684-2100-2. DOI: 10.1007/978-1-4684-2100-2_18 (cit. on p. 38).

[Mit77] A. R. Mitchell. *Computational Methods in Partial Differential Equations.* Introductory Mathematics for Scientists and Engineers. Toronto, CA: John Wiley and Sons, 1977. 255 pp. OCLC: 301599367 (cit. on p. 34).

[ML90] M. S. Mohamed and J. C. Larue. “The Decay Power Law in Grid-Generated Turbulence”. *Journal of Fluid Mechanics* 219 (Oct. 1990), pp. 195–214. ISSN: 0022-1120. DOI: 10.1017/S0022112090002919 (cit. on pp. 15, 16).

[Pra88] F. Prause. “Zerfall Des Turbulenten Strahles [Breakup of the Turbulent Jet]”. Student project. Darmstadt, Germany: TU Darmstadt, 1988 (cit. on p. 4).

[Ray78] J. W. S. Rayleigh. “On The Instability Of Jets”. *Proceedings of the London Mathematical Society* 10(1) (Nov. 14, 1878), pp. 4–13. ISSN: 1460-244X. DOI: 10.1112/plms/s1-10.1.4 (cit. on pp. 2, 13).

[RT75] A. J. Reynolds and H. J. Tucker. “The Distortion of Turbulence by General Uniform Irrotational Strain”. *Journal of Fluid Mechanics* 68(4) (Apr. 1975), pp. 673–693. ISSN: 0022-1120. DOI: 10.1017/S0022112075001176 (cit. on pp. 15, 18).

[SA10] J. H. Spurk and N. Aksel. *Fluid Mechanics*. Berlin; Heidelberg: Springer, 2010. ISBN: 978-3-642-09267-1 (cit. on pp. 5, 25).

[Sch87] H. T. Schlichting. *Boundary-Layer Theory*. Trans. by J. Kestin. 7th ed. McGraw-Hill Classic Textbook Reissue Series. New York: McGraw-Hill, 1987. 817 pp. ISBN: 978-0-07-055334-7 (cit. on pp. 5, 15).

[SS75] A. M. Sterling and C. A. Sleicher. “The Instability of Capillary Jets”. *Journal of Fluid Mechanics* 68(3) (Apr. 1975), pp. 477–495. ISSN: 0022-1120. DOI: 10.1017/S0022112075001772 (cit. on p. 14).

[Tor89] P. A. Torpey. “A Nonlinear Theory for Describing the Propagation of Disturbances on a Capillary Jet”. *Physics of Fluids A: Fluid Dynamics* 1(4) (Apr. 1, 1989), pp. 661–671. ISSN: 0899-8213. DOI: 10.1063/1.857440 (cit. on pp. 10, 27, 44).

[TR68] H. J. Tucker and A. J. Reynolds. “The Distortion of Turbulence by Irrotational Plane Strain”. *Journal of Fluid Mechanics* 32(4) (June 1968), pp. 657–673. ISSN: 0022-1120. DOI: 10.1017/S0022112068000947 (cit. on p. 16).

[Wat44] G. N. Watson. *A Treatise on the Theory of Bessel Functions*. Cambridge, UK: The University Press; The Macmillan Company, 1944. OCLC: 1109246 (cit. on p. 12).

[Web19] C. Weber. *Breakup of a Liquid Jet*. Translation. University of Texas at Austin, Oct. 20, 2019. 38 pp. DOI: 10.26153/tsw/3371 (cit. on p. 23). Trans. of “Zum Zerfall eines Flüssigkeitsstrahles [On the disintegration of a liquid jet]”. *Zeitschrift für Angewandte Mathematik und Mechanik* 11(2) (Jan. 1, 1931), pp. 136–154. ISSN: 0044-2267. DOI: 10.1002/zamm.19310110207.

[Yue68] M.-C. Yuen. “Non-Linear Capillary Instability of a Liquid Jet”. *Journal of Fluid Mechanics* 33(1) (July 1968), pp. 151–163. ISSN: 0022-1120. DOI: 10.1017/S0022112068002429 (cit. on pp. 10, 38, 40).

List of symbols

symbol	**meaning**	**dimension**[35]	
a_i	material coordinate	L	
A	anisotropy parameter	1	
A	jet cross-sectional area	L^2	
b	constant in empirical function for screen turbulence	1	
c	complex phase velocity	$L\,T^{-1}$	
c	axial strain	1	Check
c_D	nozzle contraction	1	
c_{ges}	Total strain $c \cdot c_v$	1	

[35]The dimensions are given in the basic system of mass (M), length (L), time (T).

c_v	virtual stretching	1	Check
C	general constant, empirical constant		
d	jet diameter	L	
d	wire diameter of the wire	L	
$Effekt$	measure for turbulence effect	1	
f	dimensionless velocity u/U_ref	1	
F_T	turbulence function	1	
Fr	Froude number $U^2/(gR)$	1	
g	acceleration of gravity	$\mathrm{L\,T^{-1}}$	
g	dimensionless jet radius r_s/R	$\mathrm{L\,T^{-1}}$	
G_ν	Fourier components of jet deformation	1	
i	$\sqrt{-1}$	1	
k	dimensioned wavenumber	$\mathrm{L^{-1}}$	
K_{12}	correlation coefficient	1	
L	compact jet length	L	
L	linear differential operator	$\mathrm{L^{-2}}$	
L_D	length scale of the dissipation of turbulent energy	L	
M	mesh screen size	L	
n_i, $\vec{n}$	normal vector	1	
Oh	Ohnesorge number $\nu/(\sigma R/\rho)^{1/2}$	1	
p	pressure	$\mathrm{M\,L^{-1}\,T^{-2}}$	
P	dimensionless pressure	1	
$Pegel$	measure of excitation level	1	Check
Q	density ratio between environment and jet	1	
r	radial coordinate	1	
r_s	jet radius	L	
R	undisturbed jet radius	L	
Re	Reynolds number UR/ν	1	
R_1, R_2	principal radii of curvature	L	
R_{ij}	cross-correlation of the jet edges	1	
S	turbulence parameters	1	
S_0	turbulence parameters in the isotropic case	1	
t	time	T	
T_A	anisotropy index	1	Check

T_{N}	normal stress index	1	
T_{kl}	related mean square values $\overline{u_k' u_l'}^{(0)}/U^2$	1	
Tu	turbulence intensity	1	
u	axial component of velocity	$\mathrm{L\,T^{-1}}$	
u_i'	fluctuation rate	$\mathrm{L\,T^{-1}}$	
$\overline{u_i'^2}$	mean square of the fluctuation velocity	$\mathrm{L^2\,T^{-2}}$	
U	undisturbed jet speed	$\mathrm{L\,T^{-1}}$	
$\hat{U}$	perturbation amplitude of the exit velocity	$\mathrm{L\,T^{-1}}$	
U_{ref}	reference speed $[\sigma/(\rho R)]^{1/2}$	$\mathrm{L\,T^{-1}}$	
v	radial component of the velocity	$\mathrm{L\,T^{-1}}$	
V	viscosity ratio	1	
$V_{\mathrm{K}},\ V_{\mathrm{I}},\ V_{\mathrm{I1}}$	functions in dispersion relation	1	
We	Weber number $\rho R U^2/\sigma$	1	
$\hat{\mathrm{We}}$	ambient Weber number $\hat{\rho} R U^2/\sigma$	1	
$x_i,\ \vec{x}$	position vector	L	
$y_{\mathrm{l}},\ y_{\mathrm{r}}$	jet edge coordinates	L	
$y_1,\ y_2$	jet edge displacements	L	
Y_{A}	related antisymmetric deformation content	1	Check
Y_{S}	related symmetric deformation component	1	
z	axial coordinate	L	
z_{S}	screen interval	L	
z_0	screen distance correction	L	Check
$\alpha_r,\ \alpha_z$	development coefficients of the turbulence model	1	
α_{ijkl}	coefficient matrix for the change of turbulence	1	
β	temporal growth rate	$\mathrm{T^{-1}}$	Check
δ	boundary layer thickness	L	
δ_{ij}	Kronecker-Delta (exchange symbol)	1	
ζ	dimensionless axis coordinate z/R	1	
ζ_{S}	mesh resistance coefficient	1	
η	deformation of the jet radius in linear theory	L	
η_0	initial radial displacement	L	
Θ	relative unobstructed screen surface	1	
κ	dimensionless mean curvature	1	

λ	wavelength of surface disturbances	L	Check
Λ	stability parameter	1	
$\mu_r,\ \mu_z$	functions of Rapid Distortion Theory	1	
ν	kinematic viscosity	$L^2\ T^{-1}$	
ξ	dimensionless wavenumber kR	1	
ξ_c	dimensionless cut-off wave number at FFT	1	
ξ_{grenz}	upper limit of the unstable wavenumber range	1	
π	circle number 3.1415 . . .	1	
ρ	density of the jet	$M\ L^{-3}$	
$\hat{\rho}$	density of the environment	$M\ L^{-3}$	
σ	capillary tension	$M\ T^{-2}$	
τ_{ij}	stress tensor incl. turbulent apparent stresses	$M\ L^{-1}\ T^{-2}$	
τ_{ref}	reference time $(\rho R^3/\sigma)^{1/2}$	T	
φ	part of the stream function Ψ	1	
χ	$(2We + 1 - S)/(2We)$	1	
Ψ	stream function for rotationally symmetric flow	$L^3\ T^{-1}$	
$\omega_i,\ \vec{\omega}$	fluid angular velocity	T^{-1}	Check
Ω	excitation angular frequency	T^{-1}	Check

Subscripts

i, j, k, l	general indices
min, max	at the location of a wave valley or wave crest
M	in the center of the considered jet length range
0	at the nozzle outlet
r, z	component in r or z direction or derivative with respect to r or z
t	derivation by time
φ	component in the circumferential direction

Superscripts

$^{(0)}$	undisturbed part (base flow part)
$^{(1)}$	disturbance component
$^{+}$	with U and R dimensionless

*	made dimensionless with U_{ref} (or τ_{ref}) and R
$\hat{}$	formed with the material sizes of the surrounding medium Check
-	averaged main value of a random variable
$(\,)'$	derivation according to function argument (spatial coordinate)
$(\dot{})$	derivation according to function argument (time coordinate)

Abbreviations

fcn	general indefinite function
FFT	Fast Fourier Transformation
m.Ts.	with turbulence screen
o.Ts.	without turbulence screen
$O(\,)$	order of magnitude
RDT	Rapid Distortion Theory
RMS	Root Mean Square